NACA RM E55A04

NACA

RESEARCH MEMORANDUM

EFFECTS OF INLET-AIR-FLOW DISTORTION ON STEADY-STATE ALTITUDE PERFORMANCE OF AN AXIAL-FLOW TURBOJET ENGINE

By E. William Conrad, Morgan P. Hanson, and John E. McAulay

Lewis Flight Propulsion Laboratory
Cleveland, Ohio

NATIONAL ADVISORY COMMITTEE FOR AERONAUTICS

WASHINGTON

September 27, 1955

NATIONAL ADVISORY COMMITTEE FOR AERONAUTICS

RESEARCH MEMORANDUM

EFFECTS OF INLET-AIR-FLOW DISTORTION ON STEADY-STATE ALTITUDE PERFORMANCE OF AN AXIAL-FLOW TURBOJET ENGINE

By E. William Conrad, Morgan P. Hanson, and John E. McAulay

SUMMARY

The effects of inlet-air-flow distortion on the steady-state performance of a current axial-flow turbojet engine were studied in an NACA altitude test chamber at altitudes from 15,000 to 50,000 feet at a simulated flight Mach number of 0.8. Radial distortions of various shapes up to 22 percent of the average engine-inlet total pressure and circumferential distortions up to 26 percent were imposed. Data were obtained for operation with the variable-position inlet guide vanes in both the open and closed positions with rated exhaust-nozzle area and for the exhaust nozzle open with the guide vanes in the open position.

Percentagewise, the pressure distortions were reduced markedly in passing through the compressor; however, the distortions created temperature gradients that persisted through the turbine.

The effect of inlet distortions on maximum thrust was found to be different for the two identical engines used in this study. On one engine, the maximum thrust was reduced 14 percent as a result of a reduction in engine speed required to avoid damage to the turbine-inlet stators from local overheating when the distortions were imposed. The effects on the other engine were smaller, and it was found that the amount of such derating required depends upon the turbine temperature pattern when operating with no distortion.

At intermediate engine speeds, the compressor efficiency and air flow with open inlet guide vanes were markedly reduced with radial distortions, and surge occurred at steady-state operating conditions in most cases. This area of serious difficulty, however, is normally avoided in flight by the controlled schedule of guide-vane position as a function of engine speed.

As a result of the inlet-air-flow distortions, the maximum measured value of vibratory stress in the compressor first-stage rotor blades was increased from ±15,000 to ±27,000 pounds per square inch. For both distorted and undistorted cases, the high stresses were excited by the occurrence of rotating stall.

INTRODUCTION

In virtually every submerged turbojet-engine installation, the inlet-air duct must be designed to pass around the cockpit or other items of equipment. This results in the duct having curves and bends which, in turn, may cause separation of the flow. Flow separation may also occur in either submerged or nacelle-type installations at off-design mass-flow ratios or high angles of attack. These regions of flow separation result in nonuniform distribution or distortion of the air flow entering the compressor. In addition to the large performance losses associated with the reduction in average pressure recovery (which may easily be calculated), the internal performance of the engine may also be reduced.

In the first study on air-flow distortion conducted at the NACA Lewis laboratory (ref. 1), the distortion effects were found to be negligible for the range of conditions covered; however, a subsequent study using larger distortions on a different engine (ref. 2) showed net-thrust losses on the order of 25 percent. In view of these serious losses, a continuing program was instituted to assess the effects of air-flow distortion on various engines. The effects of different shaped circumferential distortions on a third engine are given in references 3 and 4. The study reported herein is concerned with the effects on performance and compressor blade vibratory stresses of a fourth current production engine.

On the basis of existing data pertaining to air-flow distortion in flight, it was not possible to decide upon a generalized shape or pattern of pressure distribution for the tests. Accordingly, it was decided to study the effects of the following types of pressure profile:

(1) Uniform (to afford a basis of comparison)

(2) Radial (low pressure near compressor blade tips)

(3) Inverse (low pressure near compressor blade hub)

(4) Circumferential (pressure variation around circumference of compressor inlet)

(5) Mixed (combinations of 2, 3, and 4)

The largest distortions, 22-percent radial and 26-percent circumferential, were slightly larger than those expected in flight, excluding some isolated cases resulting from unusual operating conditions. The performance of the subject engine with a uniform inlet pressure profile is given in reference 5.

The effects of distortion were assessed with respect to compressor surge limits, aerodynamic conditions within the engine, component performance, over-all engine performance, and compressor blade vibration. The first two items are discussed in reference 6, and the last three are covered herein with sufficient aerodynamic information to aid in explaining the observed results.

The variable inlet guide vanes of the engine used for this study were scheduled to move from a closed to an open position at an intermediate engine speed. For this study, however, data were obtained over a complete range of corrected engine speeds with both open and closed guide vanes. With the guide vanes open, data were also obtained with the exhaust nozzle open as well as at the rated area. The investigation covered a range of altitudes from 15,000 to 50,000 feet at a flight Mach number of 0.8.

ENGINE AND INSTALLATION

The engine used in this investigation is shown in figure 1 installed in the altitude test chamber. The engine is in the 9000-pound-thrust class with a rated speed of 7950 rpm and a rated turbine-outlet temperature of 1185° F. It was comprised of a 12-stage axial-flow compressor, a cannular combustor with 10 can-type liners, a two-stage turbine, and an exhaust nozzle. A variable-area exhaust nozzle was used during the study reported herein. The important compressor parameters are:

Inlet hub-tip ratio	0.455
Pressure ratio at rated conditions	7.0
Air flow at rated speed, lb/sec	142
Rated engine speed, rpm	7950

In order to provide ample surge margin at reduced engine speeds, the engine was equipped with variable-position inlet guide vanes which rotated 30° from the closed to open position. The guide vanes were scheduled to begin opening at 6000 to 6300 rpm and to reach the open position at 7000 to 7300 rpm; the opposite was true as the speed decreased. For this investigation, however, manual operation of the vanes was substituted.

Because an instrumentation failure extensively damaged one engine part way through the investigation, a second engine of the same production configuration was used to complete the program. Slight differences in performance and distortion effects were found, and the engines are therefore designated when specific results are given.

As shown in figure 2, the engine was mounted on a thrust stand in a 14-foot-diameter altitude test chamber. High-pressure ram air was brought to the engine by means of a bellmouth inlet and a duct which passed through the front bulkhead and connected directly to the engine inlet (fig. 3). A labyrinth seal between the duct and the bulkhead was used to permit engine thrust measurement. The front bulkhead separated the high-pressure ram air from the low-pressure environment being maintained in the test chamber around the engine. Dry refrigerated air was supplied to the engine from the facility air supply system.

INSTRUMENTATION

Steady-state instrumentation used to determine the component and over-all performance was installed at the stations indicated in figure 3. Details of the instrumentation locations are given in figure 4. Pressures were measured on alkazene, water, or mercury-filled manometers and were photographically recorded. Temperatures below 700° F were measured by iron-constantan thermocouples; higher temperatures were measured with chromel-alumel thermocouples. Fuel flow was measured by the use of calibrated impeller-type flowmeters, and the values were periodically checked by means of rotameters.

Qualitative measurements of air-flow fluctuations associated with stall and surge were obtained with hot-wire anemometers that were installed at variable immersions in the 1st, 6th, and 12th stator rows of the compressor. The signals, which are functions of local mass flow, were recorded on high-speed photographic paper by a multiple-channel recorder. This instrumentation was not calibrated to give quantitative data.

Rotor-blade stresses in the 1st and 6th stages were determined with the device described in reference 3. This device comprised a magnet mounted in the tip of a rotor blade and a coil of wire on the inside of the compressor casing in the plane of rotation. Vibration of the blade produced variations in the flux and hence in the output signal from the coil. This signal, calibrated statically with an identical blade, was recorded on the multiple-channel oscillograph. The output of the strain gages on the stator blades in stages 1, 3, 5, 7, 9, and 11 was similarly recorded.

PROCEDURE

The distortions were produced by various combinations of screens installed in a plane 17 inches ahead of the inlet guide vanes. The fine mesh screen segments or rings were supported on a 1/4-inch mesh screen which covered the entire flow annulus. The 1/4-inch screen

was, in turn, supported by a number of 1/8- by 1-inch steel struts. The mesh sizes and shapes needed to give the desired distortion were determined by trial and error. Average ram or inlet pressure was based on the average readings of 64 total-pressure tubes behind the screen at the compressor inlet. Inlet pressure was set to simulate complete ram-pressure recovery at a flight Mach number of 0.8.

Complete engine performance data were obtained with no distortion and with each distortion (unless noted) over a range of corrected engine speeds from about 4800 to 8000 rpm at the following conditions:

Altitude, ft	Flight Mach number, M	Inlet-guide-vane position	Exhaust-nozzle area
35,000	0.8	Open	Rated
35,000	0.8	Open	Open
35,000	0.8	Closed	Rated
[a]15,000	0.8	Open	Rated
[a]50,000	0.8	Open	Rated

[a]Not obtained with engine 1.

During the program it was discovered that the direction of change (increasing or decreasing speed) affected the data. Accordingly, each operating line was obtained thereafter with half of the data points obtained in an increasing-speed direction and half in a decreasing-speed direction. The rated position of the exhaust nozzle was taken as that which produced military temperature at rated speed with no distortion at an altitude of 35,000 feet and a flight Mach number of 0.8. The open position of the exhaust nozzle corresponded to an area 13 percent greater than the rated area. Inlet-air temperature varied from 20° to 70° F; however, all data are adjusted to standard pressure and temperature values unless noted. Throughout the program the fuel used was MIL-F-5624A grade JP-4.

As mentioned in the INTRODUCTION, no general shape or pattern was found in existing data to simulate the various distortions existing in present airplanes or expected on the basis of model tests. With the exception of unusual operating conditions (such as a twin-pod installation at supersonic speed with one engine inoperative), a maximum distortion of 15 percent for subsonic flight and 20 percent for supersonic flight covered the great majority of the cases. In order to provide a systematic basis for the investigation, four distortion shapes were selected as follows:

(1) Circumferential (pressure variation around circumference of compressor inlet)

(2) Radial (low pressure near blade tip)

(3) Inverse (low pressure near blade hub)

(4) Mixed (combinations of 1, 2, and 3)

The shapes of the distortions produced by the screens are shown in figure 5 for operation at rated corrected engine speed. The circumferential distortions (fig. 5(a)) were intended to have a sinusoidal shape. Despite the poor simulation, the shape factor was not considered sufficiently important to warrant further attempts at achieving a better sinusoidal profile. The radial and inverse distortion shapes, figure 5(b), were varied somewhat in the spanwise direction.

Inasmuch as the pressure drop across a screen is a function of air flow, the magnitude of the distortions varied with engine speed as shown in figure 6. This variation with speed is probably different than the trends obtained with installed engines where distortions are strongly affected by duct inlet velocity ratio or shock systems. Thus the distortion existing at each speed should be borne in mind when the effects of these distortions over a range of speeds are considered.

To aid in identification of the distortions during the remainder of the report, an identification system composed of a letter and a number has been chosen. The letter denotes the shape of the distortion, and the number denotes the magnitude at rated corrected engine speed. Thus R-17 denotes a radial distortion having a pressure variation of 17 percent at rated speed. The distortions covered by this investigation are given in the following table:

No.	Type	Engine	Distortion shape
C-21	Circumferential	1	See fig. 5
C-26	Circumferential	1 and 2	See fig. 5
R-11	Radial	2	See fig. 5
R-13	Radial	1 and 2	See fig. 5
R-17	Radial	1	Similar shape to R-11
R-22	Radial	1	Similar shape to R-11
I-14	Inverse	2	See fig. 5
I-16	Inverse	2	See fig. 5
M-12	Mixed	2	Similar radial shape to I-16 in distortion area
M-15	Mixed	1	Similar radial shape to R-11 in distortion area

RESULTS AND DISCUSSION

Because of the exploratory nature of the investigation, a large quantity of data was taken. All the data were plotted and carefully examined, and the over-all effects on performance are given. However, only those data that show significant trends are discussed in detail. The main body of the report has been arranged to answer the following questions in order:

(1) How far through the engine are distortion effects propagated?

(2) What are the effects on compressor interstage performance and stall characteristics?

(3) What are the effects on over-all component performance?

(4) What are the effects on over-all engine performance?

(5) What are the effects on compressor blade vibratory stress?

Propagation through engine. - Typical effects of various distortion shapes on the temperature and pressure profiles at the compressor inlet and outlet and the turbine outlet are shown in figures 7 and 8. These data represent operation at about rated engine speed with rated exhaust nozzle and open inlet guide vanes. In order to demonstrate the effect of imposing the distortions, the data are presented in terms of the ratio of local to average pressure with distortion divided by a similar ratio without distortion. Temperatures are treated similarly.

It is seen from figure 7 that the large circumferential pressure distortion existing at the compressor inlet nearly disappeared in passing through the compressor. Similarly, the pressure profile at the turbine outlet showed a total variation of only 2 percent. Each symbol represents the average value from four radial rakes. The introduction of the distortion, however, produced a 7-percent variation circumferentially in the compressor-outlet temperature. This temperature distortion was probably largely the result of the circumferential variation in compressor pressure ratio present with the distortion. The temperature pattern increased slightly to 9 percent in amplitude in passing through the combustor and turbine. Similar effects are noted in references 2 to 4 on different engines.

The propagation of radial and inverse distortions through the engine is shown in figure 8. It should be noted that much larger scales are used at the compressor outlet and turbine outlet than at the compressor inlet. For the radial distortion, the pressures at the compressor outlet were virtually the same as for no distortion. The 16-percent inverse distortion produced only about a 1-percent change in total

pressure at the compressor outlet. In neither case were pressures at the turbine outlet appreciably affected. Hence, for all practical purposes, the pressure distortion in both cases disappears in the compressor. Just as in the case of the circumferential distortion, temperature gradients were produced at the compressor outlet which were identifiable with the distribution of compressor pressure ratio. The size of the temperature distortion, however, was much smaller than that produced by the circumferential distortion. The maximum change in profile at the compressor outlet was an increase of 1.6 percent and occurred with the radial distortion. The maximum change at the turbine outlet was about 2.3 percent, occurring with the inverse distortion.

The ratio parameters used in figures 7 and 8 were selected to illustrate the shifts in profile resulting from the distortion. In the consideration of materials, however, the absolute temperature values at the turbine are of more importance than the shift. The effects of these distortions on engine performance as limited by high local temperatures will be discussed in a later section.

In figures 7 and 8, it is seen that the pressure distortions largely disappeared in passing through the compressor while slight shifts in temperature were produced. In order to show the extent of these profiles within the compressor, interstage data are presented in figure 9. It is seen that both radial and inverse distortions in pressure have disappeared within the first four stages. It is probable that most of the distortion disappeared in the first or second stage; however, instrumentation was not adequate to confirm this belief. Early in the compressor, the radial distortion produced a slight increase in temperature near the tip which persisted to the compressor outlet. This temperature increase probably results from the increase in pressure ratio near the tip in the first few stages. The inverse distortion produced no significant shift in interstage temperature distribution.

Compressor-interstage performance and stall. - The compressor-interstage performance and stall characteristics are of interest in providing some insight into the reasons for the observed effects of distortion on the over-all performance of the compressor. In order to illustrate the effects of inlet distortion on the interstage performance and stall characteristics, it is necessary to review briefly some of the characteristics of the compressor with no distortion reported in references 6 and 7. Although operation with the guide vanes open at low engine speeds does not occur in controlled-engine operation because of the guide-vane schedule used, the compressor characteristics in this area are of considerable interest to those engaged in compressor design and, hence, are given full consideration.

As shown by the discontinuities in figure 10, three distinct modes of operation occur with the inlet guide vanes in the open position. At corrected speeds below about 5800 rpm, the compressor is in tip stall (stall at tips of blades in compressor stages 1 to 4). In the speed range from approximately 5800 to about 6600 rpm, rotating stall exists and at higher speeds operation is stall-free. The rotating stall consists of one stalled area near the tip rotating at 0.50 of the engine speed. This rotating-stall mode of operation appears to be a transition between the other two regions. The overlap of the segments is due to hysteresis. When speed is gradually decreased from rated, stall-free operation persists to a speed of 6200 rpm before rotating stall suddenly commences; however, when speed is gradually increased in the rotating-stall region, stall-free operation does not occur until a speed of 6550 rpm is reached. Decreases in Reynolds number (increases in altitude) caused the rotating-stall zone to shift to slightly higher speeds and to exist over a narrower speed range.

As shown by the dashed line, operation with the inlet guide vanes closed eliminated both rotating stall and tip stall in this range of speeds, resulting in a single continuous operating line. Closing the guide vanes resulted in both higher air flow and efficiency at low engine speeds. The effects of inlet-guide-vane position on the characteristics of this engine are discussed in detail in reference 8. Inasmuch as the guide vanes are scheduled to modulate from closed to open in the speed range from about 6000 to about 7000 rpm, the schedule would avoid both stall regions during normal engine operation except under unusual conditions such as a very hot (100° F) day at sea level, Mach 0.75, and an uncorrected engine speed of 7000 rpm. Thus, the open-guide-vane characteristics at low speeds are primarily of interest to those concerned with compressor or control design.

The effects of radial and inverse distortions on the characteristics of the first group of stages (1 to 4) are shown in figure 11, where the pressure coefficient is plotted as a function of the flow coefficient. With closed inlet guide vanes (fig. 11(b)) the characteristics are very similar for operation with no distortion or with a radial distortion, the only exception being the reduced pressure coefficient for the lowest speed point with radial distortion. This reduction may indicate the presence of stall within the stage group. The inverse distortion caused a shift to both higher pressure coefficient and flow coefficient for operation at constant corrected engine speed. The explanation for this shift probably lies in a shift in the blade-element loading along the span; however, analysis is not possible because the necessary assumption of radial equilibrium of the flow leaving the inlet guide vanes is probably not valid in the presence of these distortions. It is significant that no discontinuities or breaks occurred in these characteristic curves.

In contrast, sharp breaks are apparent in all three curves for operation with the inlet guide vanes open (fig. 11(a)). These breaks are due to the occurrence of rotating stall and tip stall just discussed. The region of rotating stall is denoted by the shaded area. Broken lines and arrows are used to denote hysteresis associated with direction of approach. There is little effect of distortion at either high speeds (stall-free) or low speeds (tip stall); however, the distortion caused a shift in the speed range occupied by rotating stall. The radial distortion shifted the region of rotating stall to higher speeds, resulting in a peak pressure coefficient of 0.30 at a corrected speed of 6600 rpm as compared with a value of 0.32 at 6000 rpm for the undistorted case. The inverse distortion had the opposite effect, shifting the region of rotating stall to a lower speed range and allowing higher peak values of pressure coefficient. With the inverse distortion, the peak pressure coefficient was 0.336.

Because of the serious effect of the radial distortion shown in figure 11 with open guide vanes, the effect of radial distortion on the blade-element characteristics was examined throughout the remainder of the compressor. The most significant effect was found in stages 8 to 10, although it may have been due to cumulative effects in earlier stages.

In figure 12 are shown typical effects of radial distortions on the blade-element performance characteristics of this group. In the direction of increasing speed shown by the solid line in figure 12(b), the root-element performance deteriorates very rapidly in the rotating-stall region at speeds above about 6700 rpm where the distortion amplitude was 7 percent. This deterioration is accompanied by the appearance of a very severe rotating-stall segment at the roots in the sixth stage which does not occur for no distortion or inverse distortion. Further, very gradual increases in engine speed result in severe surge during essentially steady-state conditions at a speed of 7100 rpm where the amplitude of the distortion was 9 percent. Higher speeds cannot be obtained without guide-vane adjustment. This speed limitation would limit the thrust of the engine to about 38 percent of the rated value if encountered in flight; however, because of the guide-vane schedule used, it will occur rarely, if at all, for the amplutudes (including speed effect (fig. 6)) and shapes investigated. In regard to this limitation of speed due to surge at steady-state conditions, four other observations are noteworthy:

(1) The limitation did not always occur with radial distortions having an amplitude of 17 percent or less at rated speed.

(2) The limit was avoided by setting the guide vanes only a few degrees closed.

(3) By closing the guide vanes, going to rated speed, and then opening the guide vanes, normal operation was obtained over the speed range from corrected speeds of 6800 to 8000 rpm (broken curves of fig. 12(b)).

(4) The undistorted engine showed tendencies to border on this condition of surge at an altitude of 50,000 feet.

Effects on component performance. - A careful examination of the data on combustor and turbine characteristics showed no discernible effect of distortion on the performance of these components, although the compressor performance was affected. Accordingly, only the data on compressor characteristics will be shown. Typical data are shown in figures 13(a) and (b) for the following operating conditions: inlet guide vanes open; altitude, 35,000 feet; flight Mach number, 0.8; and direction of speed change, increasing. It is seen that the data separate into two distortion groups: (1) radial and mixed radial and (2) circumferential, inverse, and undistorted. Over most of the speed range covered, group 1 exhibits lower air flows and much lower efficiencies than group 2, and the occurrence of surge prevents operation at corrected speeds above about 7100 rpm. This trend is, of course, to be expected from the severe rotating stall at the roots of the sixth stage, as discussed in connection with figure 12(b).

In all cases during this investigation the performance with mixed distortions behaved according to the trend of performance with the radial component, that is, a mixed distortion of the circumferential and radial type would affect performance in the same manner as a pure radial distortion. Performance with group 2 (circumferential and inverse distortion) follows the trend of performance with the undistorted configuration. Even though the radial component of a mixed distortion had the predominant effect on the engine investigated, it should be noted that other engines may be more susceptible to circumferential than radial distortions. In such an engine, the effects of a mixed distortion would then be governed by the circumferential component rather than the radial.

As noted earlier, operation at rated speed was possible with the radial distortion if the guide vanes were closed to allow acceleration and then opened at high speed. The data then obtained in the order of decreasing speed, figures 13(c) and (d), show somewhat lower efficiency at high speed for the radial distortions but about the same air flow as the undistorted case. At speeds below about 6600 rpm, the trends are similar to those for increasing speed.

The typical effects of radial and inverse distortions on the compressor characteristics with the inlet guide vanes closed are given in figure 14 for operation at an altitude of 35,000 feet and a flight Mach number of 0.8. Because of the elimination of both rotating stall and

[redacted]

tip stall by closing the guide vanes, no discontinuities occur. The only significant effects of these distortions are (1) with the inverse distortion there is a slight increase in efficiency at low engine speeds and small increase in air flow at all speeds and (2) with the radial distortion there is a decrease in efficiency at high speeds and very low speeds.

Effects on over-all engine performance. - In regard to over-all engine performance, perhaps the most significant question is, "What are the effects of various distortions on the maximum safe thrust and on the corresponding specific fuel consumption?" From the relatively small effects of distortion on the component performance, as discussed in the last section, it might be expected that the predominant effect on maximum thrust would be associated with the shift in temperature profile at the turbine, as shown in figure 7. The circumferential shift shown in figure 7 was much larger than the change in average radial temperature profile shown in figure 8. Thus it is likely that the turbine stator diaphragm would be more adversely affected than the turbine rotor blades by the introduction of a distortion at the engine inlet. It should be noted that the radial and inverse distortions also produced circumferential temperature shifts similar to the effect shown in figure 7. The stator diaphragm, then, rather than the rotor blades would be expected to impose a limit on the maximum safe bulk gas temperature at the turbine.

As discussed in reference 3, shifts in the turbine temperature profile, resulting from distortions in the flow at the engine inlet, can produce local areas of excessive temperature and destroy the turbine stator diaphragm. Accordingly, corrected engine speed, corrected net thrust, and corrected specific fuel consumption are shown for the various distortions as functions of the local maximum gas temperature at the turbine outlet in figure 15. Turbine-inlet temperature should, of course, be used to indicate safe turbine operating conditions; however, because of the difficulty in obtaining accurate measurements at the turbine inlet, measurements at the turbine outlet were used. Experience with other engines has indicated that temperature peaks are usually attenuated in passing through the turbine. Accordingly, the required performance derating shown in figure 15 is probably conservative. The quantities are expressed as percentages of the same quantities for the engine operating with no distortion, and the local maximum temperature is given as the ratio to engine-inlet temperature $\left(\frac{T_{6,max}}{T_1}\right)$ to eliminate small experimental deviations in setting the engine-inlet temperature. Data for the first engine are given in figure 15(a) and for the second engine in figure 15(b). All data are for operation with NACA standard conditions at an altitude of 35,000 feet at a flight Mach number of 0.8.

[redacted]

In general, for the first engine operating at a given local maximum temperature, engine speed, net thrust, and specific fuel consumption were reduced by the introduction of a distortion. If it is assummed that the engine cannot safely tolerate a local turbine temperature higher than that which existed with no distortion (a local temperature ratio of 3.43), the maximum safe performance with the various distortions would be as follows:

Distortion	Corrected speed, $N/\sqrt{\theta}$, percent of undistorted	Corrected net thrust, F_n/δ, percent of undistorted	Corrected specific fuel consumption, $W_f/F_n\sqrt{\theta}$, percent of undistorted
C-21	97.7	102.4	101.4
C-26	100.0	93.2	103.3
R-17	96.7	91.5	98.3
R-13	97.2	86.0	97.9
M-15	97.0	88.2	97.0

It is seen that the maximum safe thrust is reduced 14 percent for the 13-percent radial distortion. The larger derating required for safe operation with R-13 as compared with R-17 may have been due to the difference in the distortion shape. R-17 was similar in shape to R-11, which is shown along with R-13 in figure 5. The reductions with the circumferential (C-21) and mixed distortions were smaller but still substantial. The specific fuel consumption varied from 97 percent for the mixed distortion, to 102.3 for the largest circumferential at rated speed. Because the curves of figure 15(a) are more or less parallel, the absolute value of maximum local temperature assumed has little effect on the amount of derating required.

Similar data for various distortions imposed on the second engine are given in figure 15(b). If mechanical speed is limited to the rated value and the local temperature limit is restricted to the maximum value for no distortion, the maximum safe performance is as follows:

Distortion	Corrected speed, $N/\sqrt{\theta}$, percent of undistorted	Corrected net thrust, F_n/δ percent of undistorted	Corrected specific fuel consumption, $W_f/F_n\sqrt{\theta}$, percent of undistorted
R-11	99.2	98.0	100.2
R-13	98.8	95.0	100.5
I-13	100.0	100.7	100.3
I-15	100.0	100.0	102.8
C-26	100.0	100.0	100.6

[redacted]

The loss in performance with this engine is, in general, much smaller because of differences in the turbine temperature patterns of the two engines when operating with no distortion. This lack of performance reproducibility among production engines of the same make and model is well known and is attributed to the difficulty in achieving perfect balance among the fuel nozzles over a wide range of fuel flows. As an example of this effect the temperature shift resulting from the introduction of a severe circumferential distortion C-26 on the second engine merely served to "fill a valley" which existed in the temperature pattern with no distortion; whereas on the first engine, the shift produced by the 26-percent circumferential distortion increased a local temperature which was already high, thus requiring derating to allow safe engine operation. From these observations it is therefore obvious that the amount of derating required to assure safe turbine operation is dependent upon the geometric matching between the inlet distortion and the turbine temperature pattern existing with no distortion. Accordingly, the amounts of thrust derating given herein are indicative only of the amount of derating that may be required and are not necessarily either the maximum or minimum.

These data then serve only to illustrate the seriousness of the general problem of inlet-air distortion on engine performance and to show that the problem is rendered even more difficult because the effects cannot be generalized, even between engines of the same make and model. In addition, the values quoted are probably applicable only as measured by the turbine-outlet temperature survey; a still more comprehensive survey may well have disclosed other "hot spots" and hence altered these values.

The radial and inverse distortions tended to produce high local temperatures at some (but not all) circumferential positions at the turbine outlet and hence required derating to protect the turbine stator assembly. The circumferentially averaged temperature at a given radius was not seriously affected, however; hence the turbine rotor blades, which "feel" only the average value at a given radius, did not require derating of the engine to ensure safe operation.

Figure 15 may also be used to determine the effects of distortion on the specific fuel consumption at cruise conditions. For cruise operation at 90 and 80 percent of the rated thrust of the engine with no distortion, the following values of specific fuel consumption were obtained:

Engine I		
Distortion	Specific fuel consumption, percent of rated undistorted	
	90 Percent rated thrust	80 Percent rated thrust
No distortion	98.0	97.3
C-21	100.6	100.0
C-26	101.0	97.5
R-17	98.5	97.4
R-13	90 Percent thrust not possible	97.0
M-15	90 Percent thrust not possible	95.5
Engine II		
No distortion	97.5	97.0
R-11	99.2	99.2
R-13	99.7	98.7
I-13	99.4	99.2
I-15	102.5	102.3
C-26	99.5	99.2

From these tabulated values, it is seen that the effect of these distortions on the specific fuel consumption for cruise, although significant, is small. The largest variation among distortions was only about 4.5 percent.

The loiter condition of 30 percent of rated thrust (no distortion) is given in figure 16. The abscissa for each bar is based on 100 percent for the undistorted engine. Although a flight Mach number of 0.8 is not representative of a loiter condition, data were not obtained at lower Mach numbers to illustrate the effects on loiter performance; accordingly, data at 30 percent thrust (fig. 16) should be considered only as a rough indication. In this case, the maximum increase in specific fuel consumption was about 6 percent, while the maximum decrease was about 5 percent. Thus it is seen that, for the distortions investigated, performance penalties, while serious, are not of the same magnitude as those found in references 2 to 4 for other engines.

Effect on compressor blade vibration. - An examination of the stress records revealed that vibratory stress values were not serious in the stator blades nor the sixth-stage rotor blades; accordingly, the following discussion is limited to consideration of vibratory stress in the first-stage rotor blades. The sources of excitation for the first-stage rotor blades are illustrated by the data of figure 17. The calculated natural frequency of the first-stage rotor blades is shown by the solid curved line. Another solid straight line denotes the second-order curve (twice engine speed) for the engine. Two basic relative stall frequencies were obtained, and curves of four times stall frequency are denoted by the broken lines. The symbols denote the measured values of blade frequency where significant vibration was present. It will be seen that the measured frequencies agree well with the calculated natural frequency and also that the significant vibration occurred near the intersections, indicating that either rotating stall or second-order excitations could be the source mechanism.

The relative frequency of the rotating-stall segment with respect to the rotor blades is shown in figure 18(a) for steady-state operation. All data fell along a single straight line irrespective of distortion type. This line shows the relative stall frequency to be very close to one-half the engine speed. During steady-state operation, no rotating stall occurred with the guide vanes closed. Similar data obtained under transient conditions are shown in figure 18(b). Here it is seen that rotating stall at higher relative frequency did occur during transients.

In figure 19(a), values of blade vibratory stress measured near the blade root are shown for steady-state operation with open inlet guide vanes. The highest measured stress of ±23,000 pounds per square inch occurred with distortion at an engine speed of 6300 rpm indicating, from figure 17, excitation by rotating stall rather than forced second-order excitation. Peak stress with no distortion was 38 percent lower. Although no quantitative data are available, the higher stresses with distortion may possibly be explained by a larger change in mass flow (hence higher excitation energy) associated with the passage of the stall segment with respect to the blades. The data were not adequate to define a definite relation between the stress peaks and the type of distortion.

Similar data obtained during transients are presented in figure 19(b). These data definitely establish rotating stall as the exciting mechanism inasmuch as (1) peak stress values coincide with the intersection speeds of figure 17 for rotating stall, and (2) high stresses were absent where rotating stall was not present (fig. 19(a) at 5400 rpm) but were large when rotating stall was present in the same speed range (fig. 19(b)). Again in figure 19(b) it is seen that the peak stress of ±27,500 pounds per square inch occurred with distortion (not the same distortion producing the peak in fig. 19(a)) and that peak stress without distortion was 55 percent lower.

The seriousness of these stress values is difficult to determine explicitly because of superimposed centrifugal and torsional stresses (which are relatively small) and because the area of strain-gage attachment could not correspond to the exact point of maximum stress. Some appreciation of how serious these stress values are may be had by noting that steel blades have an endurance limit of about 44,000 pounds per square inch under superimposed centrifugal loading.

CONCLUDING REMARKS

From this investigation to determine the effects of various patterns of inlet-air distortion on the performance of a modern axial-flow turbojet engine (equipped with variable-position inlet guide vanes), it was found that the performance of the combustor and turbine was not appreciably affected. Percentagewise, the pressure distortions were reduced markedly in passing through the compressor; however, the distortions created temperature gradients that persisted throughout the turbine. The compressor characteristics were, however, affected by the inlet distortion, particularly for the radial and inverse distortions when the engine was operated with open inlet guide vanes. The radial distortion (low pressure at hub) increased the speed at which rotating stall was present, whereas the inverse distortion (low pressure at tip) had the opposite effect. Also, the radial distortion produced surge at steady-state conditions with the guide vanes open; however, this limitation will normally be avoided by the inlet-guide-vane schedule used. The behavior of mixed distortions was governed by the radial pressure variation rather than the circumferential variation in pressure.

In regard to over-all engine performance, the maximum effect of the distortions studied on net thrust (exclusive of inlet duct losses) was a 14-percent reduction. This reduction was primarily due to a decrease in engine speed which was necessary to avoid excessive local turbine gas temperature when operating with distortion in the engine air flow. The amounts of derating required to ensure safe turbine operation were considerably different on the two engines (of the same make and model) used in this study. Hence the derating of 14 percent must be regarded only as an indication of the seriousness of the problem of air distortion.

The maximum measured value of first-stage rotor-blade vibratory stress increased from ±15,000 to ±27,000 pounds per square inch as a result of distortion; however, these stress values are within the endurance limit of the blade material used. Rotating stall was found to be the source of excitation of the high stress values measured.

Lewis Flight Propulsion Laboratory
National Advisory Committee for Aeronautics
Cleveland, Ohio, April 21, 1955

APPENDIX A

SYMBOLS

The following symbols are used in this report:

A	area, sq ft
F_j	jet thrust, lb
F_n	net thrust, lb
g	gravitational constant, 32.2 ft/sec^2
H	enthalpy, Btu/lb
K	dimensional constant, $\frac{ft^2\text{-sec}}{lb}$
M	Mach number
N	engine speed, rpm
P	total pressure, lb/sq ft abs
p	static pressure, lb/sq ft abs
R	gas constant, 53.3 ft-lb/(lb)($^\circ$R)
T	total temperature, $^\circ$R
T_i	indicated temperature, $^\circ$R
t	static temperature, $^\circ$R
V	velocity, ft/sec
W_a	air flow, lb/sec
W_f	fuel flow, lb/hr
W_g	gas flow, lb/sec
γ	ratio of specific heats for gases
δ	ratio of engine-inlet total pressure to absolute static pressure of NACA standard atmosphere at sea level

[redacted]

η_c compressor adiabatic efficiency

θ ratio of absolute engine-inlet total temperature to absolute static temperature of NACA standard atmosphere at sea level

φ flow coefficient

ψ pressure coefficient

Subscripts:

a air

ac actual

av average

d distorted

e equivalent

ef effective

f fuel

g gas

i indicated

is isentropic

j jet

l local

t turbine

u undistorted

v vena contracta

0 free-stream conditions

1 engine inlet (ahead of screens)

2 compressor inlet

3 compressor outlet

4	combustor inlet
5	turbine inlet
6	turbine outlet
7	exhaust-nozzle inlet
8	exhaust-nozzle outlet

3544

[redacted]

APPENDIX B

REDUCTION OF EXPERIMENTAL DATA

Flight Mach number. - Because it was desired to determine the effects of distortion on the internal performance of the engine itself (ignoring losses associated with ram recovery in the inlet duct), the performance in all cases is compared at a common arithmetic average pressure at the compressor inlet, station 2 (behind the blockage screens). The equivalent flight Mach number was determined from this average pressure and the simulated altitude pressure in the test chamber p_0 by use of the expression

$$M_{0,e} = \sqrt{\frac{2}{\gamma - 1}\left[\left(\frac{P_2}{p_0}\right)^{\frac{\gamma-1}{\gamma}} - 1\right]}$$

Equivalent temperature. - Equivalent static temperature was determined from ambient static pressure and engine-inlet total pressure and temperature:

$$t_{0,e} = \frac{T_1}{\left(\frac{P_2}{p_0}\right)^{\frac{\gamma-1}{\gamma}}}$$

Airspeed. - The following equation was used to calculate airspeed:

$$V_{0,e} = M_{0,e}\sqrt{gRt_{0,e}}$$

Temperature. - Total temperatures were determined from indicated temperatures by the following relation:

$$T = \frac{T_i\left(\frac{P}{p}\right)^{\frac{\gamma-1}{\gamma}}}{1 + 0.85\left[\left(\frac{P}{p}\right)^{\frac{\gamma-1}{\gamma}} - 1\right]}$$

where 0.85 was taken as the recovery factor for the thermocouple used.

Air flow. - With uniform pressure at the engine inlet, the engine air flow was determined from pressure and temperature measurements at station 1 at the engine inlet and from the following equation:

$$W_{a,1} = A_1 p_1 \sqrt{\frac{2g\gamma}{RT_1(\gamma - 1)} \left(\frac{P_1}{p_1}\right)^{\frac{\gamma-1}{\gamma}} \left[\left(\frac{P_1}{p_1}\right)^{\frac{\gamma-1}{\gamma}} - 1\right]}$$

With the screens installed (as shown in fig. 3) it was found that even though air-flow measuring instrumentation was installed 10 inches upstream of the screens, the air-flow data were not reliable due to static-pressure gradients produced by the damming action of the screens. Accordingly, air flow with the distortions was determined from the effective flow area of the turbine nozzles. This effective flow area was determined from the relation

$$A_t = K \frac{\frac{W_{a,1}\sqrt{\theta_1}}{\delta_1}\sqrt{\frac{T_5}{T_1}}}{\frac{P_5}{p_1}}$$

where

$$K = \frac{W_{g,5}}{W_{a,1}} \frac{\sqrt{519}}{2116} \sqrt{\frac{R}{\gamma g}} \left(\frac{\gamma + 1}{2}\right)^{\frac{\gamma+1}{2(\gamma-1)}}$$

by using data for the engine with no distortion. The turbine-inlet temperature was calculated from the measured temperature at the turbine outlet and the enthalpy rise across the compressor. Reynolds number effects on the effective area were taken into account by the use of data for an identical Reynolds number index in the preceding equation. The corrected air flow for the distorted cases was then obtained by using this same expression and the effective turbine area.

Gas flow. - The weight flow of gas leaving the exhaust nozzle was calculated as follows:

$$W_g = W_a + \frac{W_f}{3600}$$

[redacted]

Net thrust. - Net thrust was obtained by determining the jet thrust and subtracting the momentum that the inlet air would have in flight. Jet thrust was based on rake measurements in the tail pipe and is given by

$$F_j = \frac{W_{g,7}}{g} V_{ef}$$

In a perfect converging nozzle,

$$V_{ef} = V_v + \frac{A_v(p_v - p_0)}{W_{g,7}/g}$$

where V_v, A_v, and p_v are the velocity, area, and static pressure, respectively, at the vena contracta. Net thrust is then given by

$$F_n = F_j - \frac{W_{a,1}}{g} V_{0,e}$$

Compressor efficiency. - Adiabatic efficiency of the compressor was based on average values of pressure and temperature before and after the compressor with the use of the following equation:

$$\eta_c = \frac{H_{3,is} - H_1}{H_{3,ac} - H_1}$$

where enthalpy values were obtained from standard tables.

REFERENCES

1. Conrad, E. William, and Sobolewski, Adam E.: Investigation of Effects of Inlet-Air Velocity Distortion on Performance of Turbojet Engine. NACA RM E50G11, 1950.

2. Wallner, Lewis E., Conrad, E. William, and Prince, William R.: Effect of Uneven Air-Flow Distribution to the Twin Inlets of an Axial-Flow Turbojet Engine. NACA RM E52K06, 1953.

3. Walker, Curtis L., Sivo, Joseph N., and Jansen, Emmert T.: Effect of Unequal Air-Flow Distribution from the Twin Inlet Ducts on Performance of an Axial-Flow Turbojet Engine. NACA RM E54E13, 1954.

4. Huntley, S. C., Sivo, Joseph N., and Walker, Curtis L.: Effect of Circumferential Total-Pressure Gradients Typical of Single-Inlet Duct Installations on Performance of an Axial-Flow Turbojet Engine. NACA RM E54K26a, 1955.

5. Kaufman, Harold R., and Dobson, Wilbur F.: Performance of YJ73-GE-3 Turbojet Engine in Altitude Test Chamber. NACA RM E54F22, 1955.

6. Harry, David P., III, and Lubick, Robert J.: Inlet-Air Distortion Effects on Stall, Surge, and Acceleration Margin of a Turbojet Engine Equipped with Variable Compressor Inlet Guide Vanes. NACA RM E54K26, 1955.

7. Wallner, Lewis E., and Lubick, Robert J.: Steady-State and Surge Characteristics of a Compressor Equipped with Variable Inlet Guide Vanes Operating in a Turbojet Engine. NACA RM E54I28, 1954.

8. Budinger, Ray E., and Kaufman, Harold R.: Investigation of the Performance of a Turbojet Engine with Variable-Position Compressor Inlet Guide Vanes. NACA RM E54L23a, 1955.

[redacted]

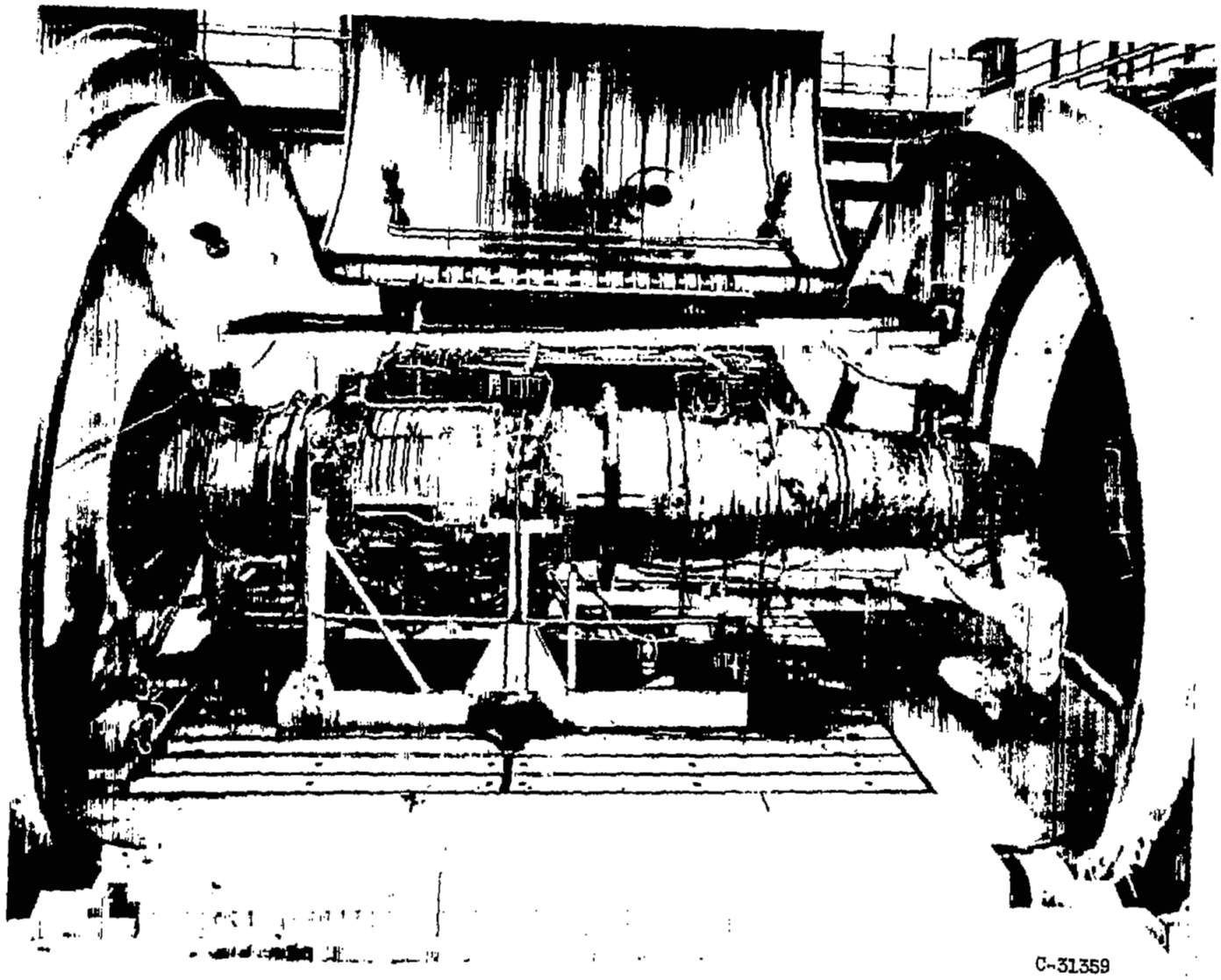

C-31359

Figure 1 - Engine installed in altitude test chamber.

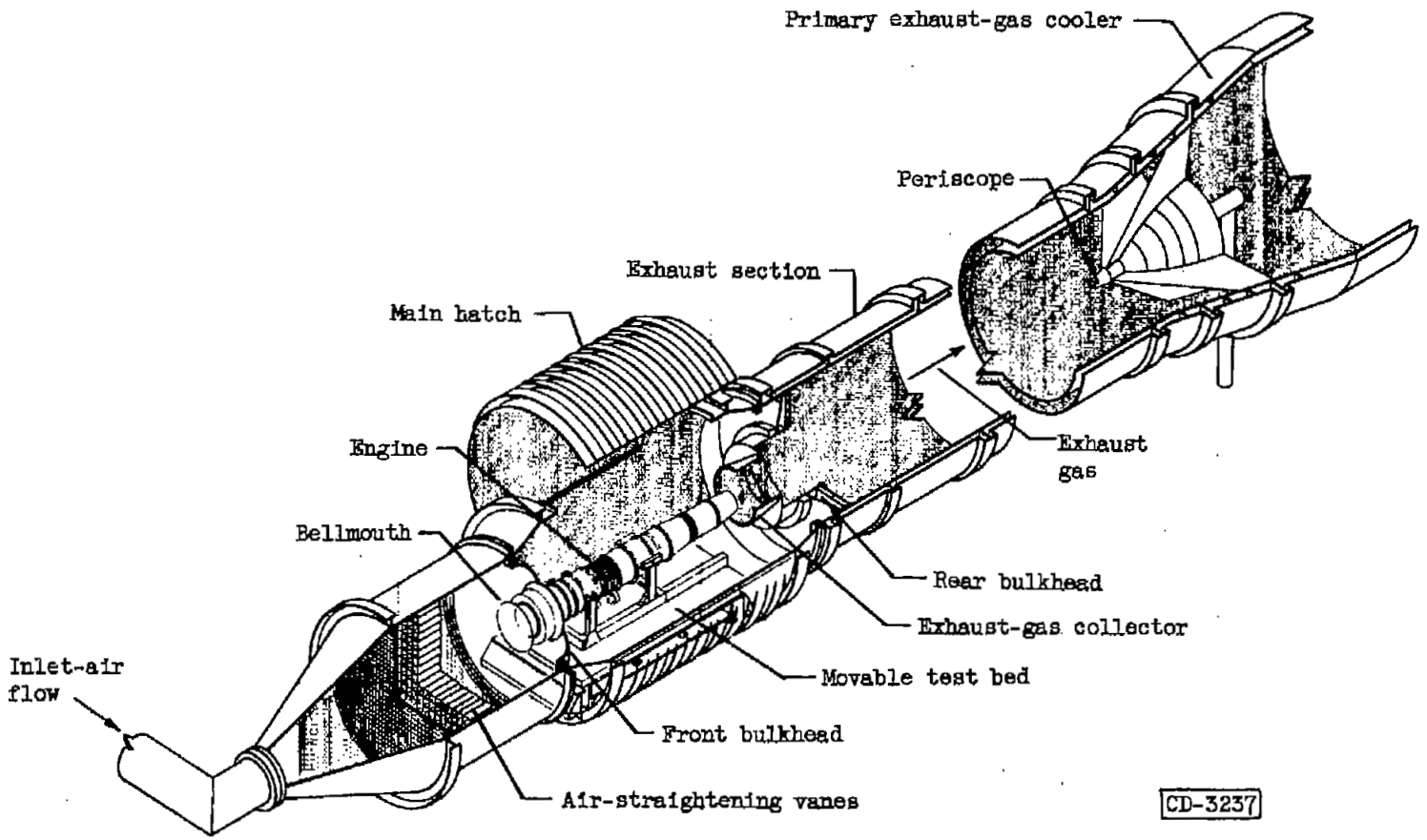

Figure 2. - Altitude chamber with engine installed in test section.

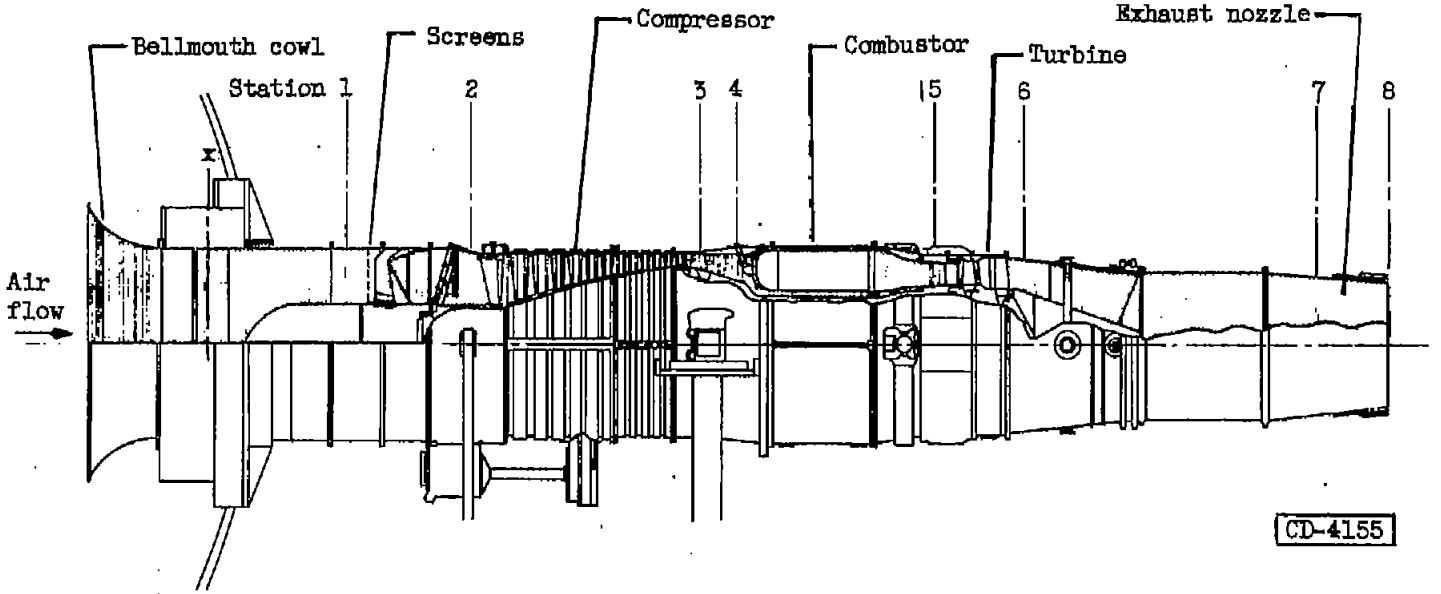

Station	Location	Total-pressure tubes	Static-pressure tubes	Wall static-pressure orifices	Thermo-couples
x		0	0	4	0
1	Engine inlet	10	16	4	16
2	Compressor inlet	63	0	0	0
3	Compressor outlet	59	0	0	49
4	Combustor inlet	5	0	0	0
5	Turbine inlet	9	0	0	0
6	Turbine outlet	24	0	8	20
7	Exhaust-nozzle inlet	28	16	4	20
8	Exhaust-nozzle outlet	0	4	0	0

Figure 3. - Cross section of turbojet engine showing stations at which instrumentation was installed.

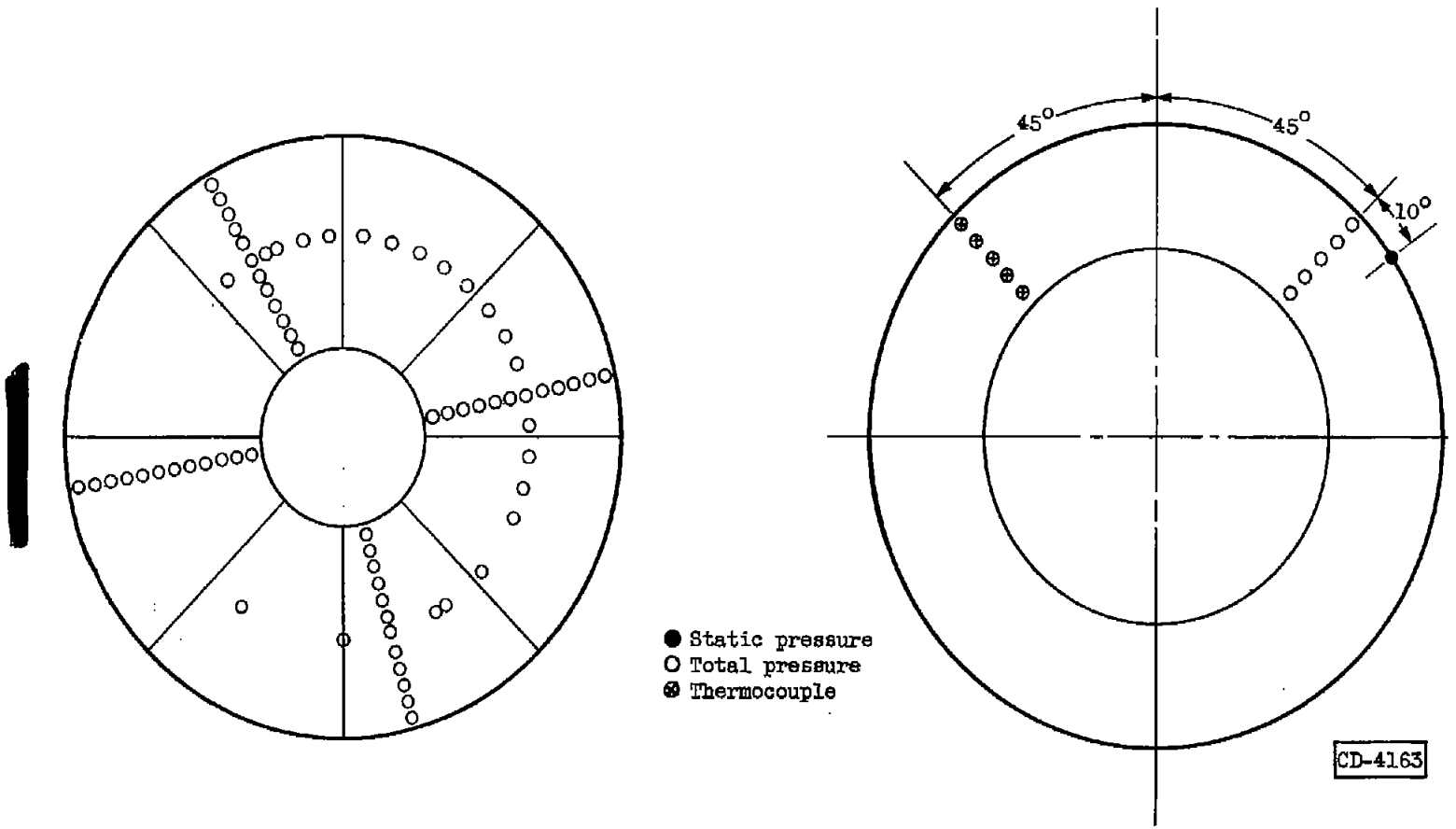

(a) Compressor inlet.

(b) Compressor interstage (stages 4,7, and 10).

Figure 4. - Details of instrumentation (looking downstream).

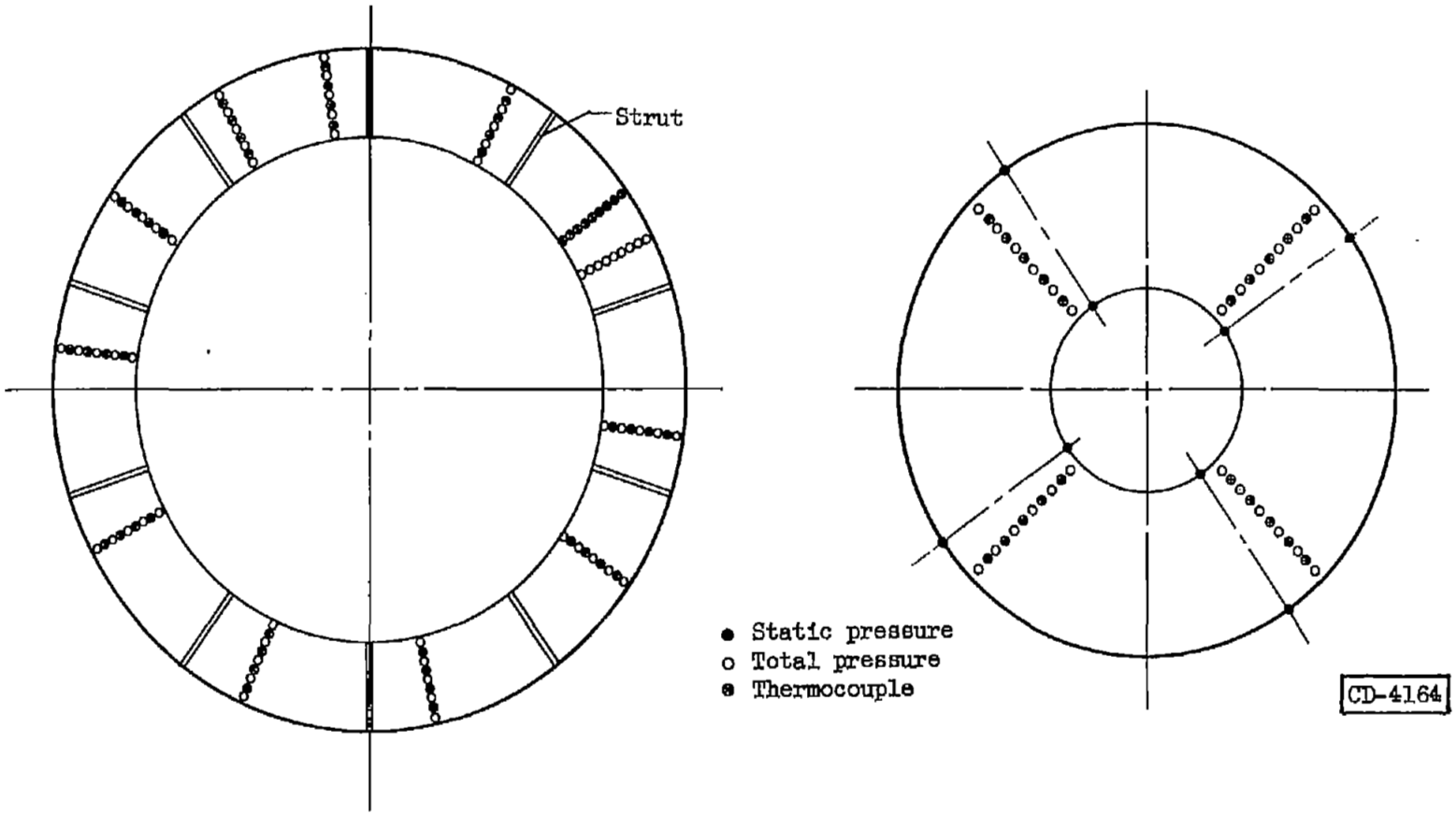

(c) Compressor outlet.

(d) Turbine outlet.

Figure 4. - Concluded. Details of instrumentation (looking downstream).

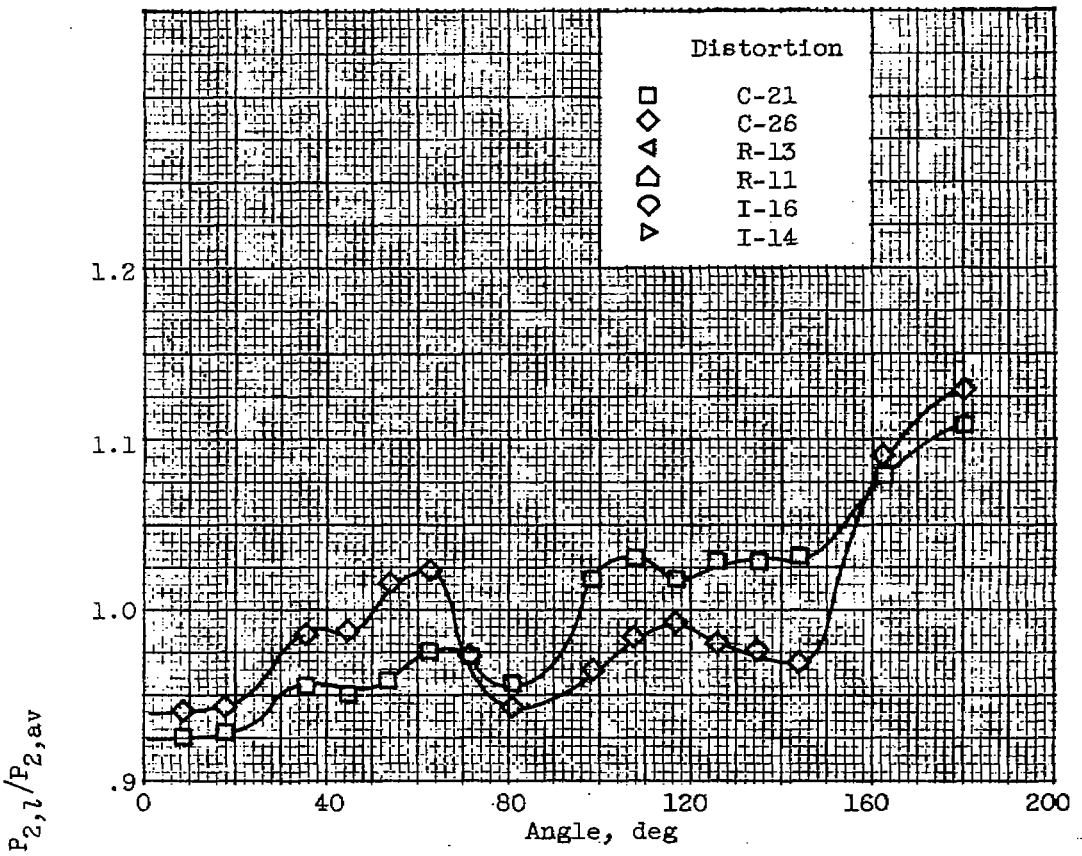

(a) Circumferential distortions.

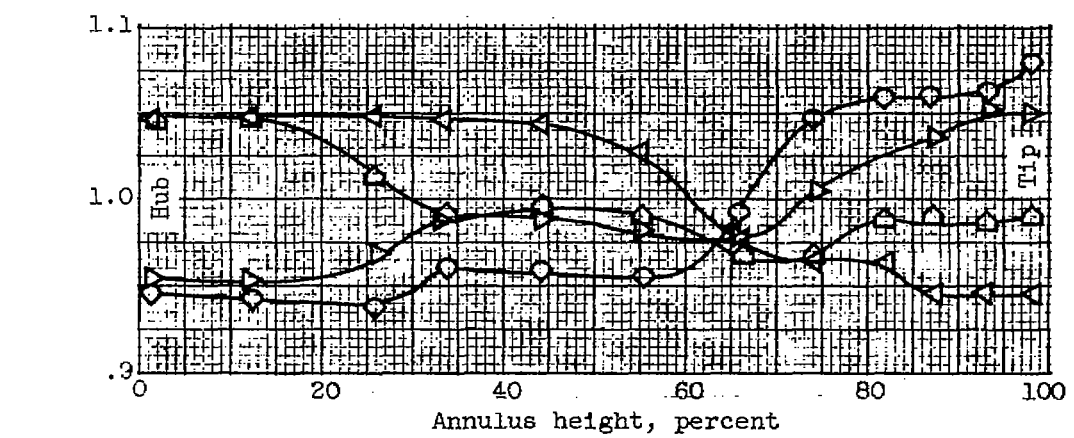

(b) Radial and inverse distortions.

Figure 5. - Pressure profiles at compressor inlet. Inlet guide vanes open; rated corrected engine speed; altitude, 35,000 feet.

[redacted]

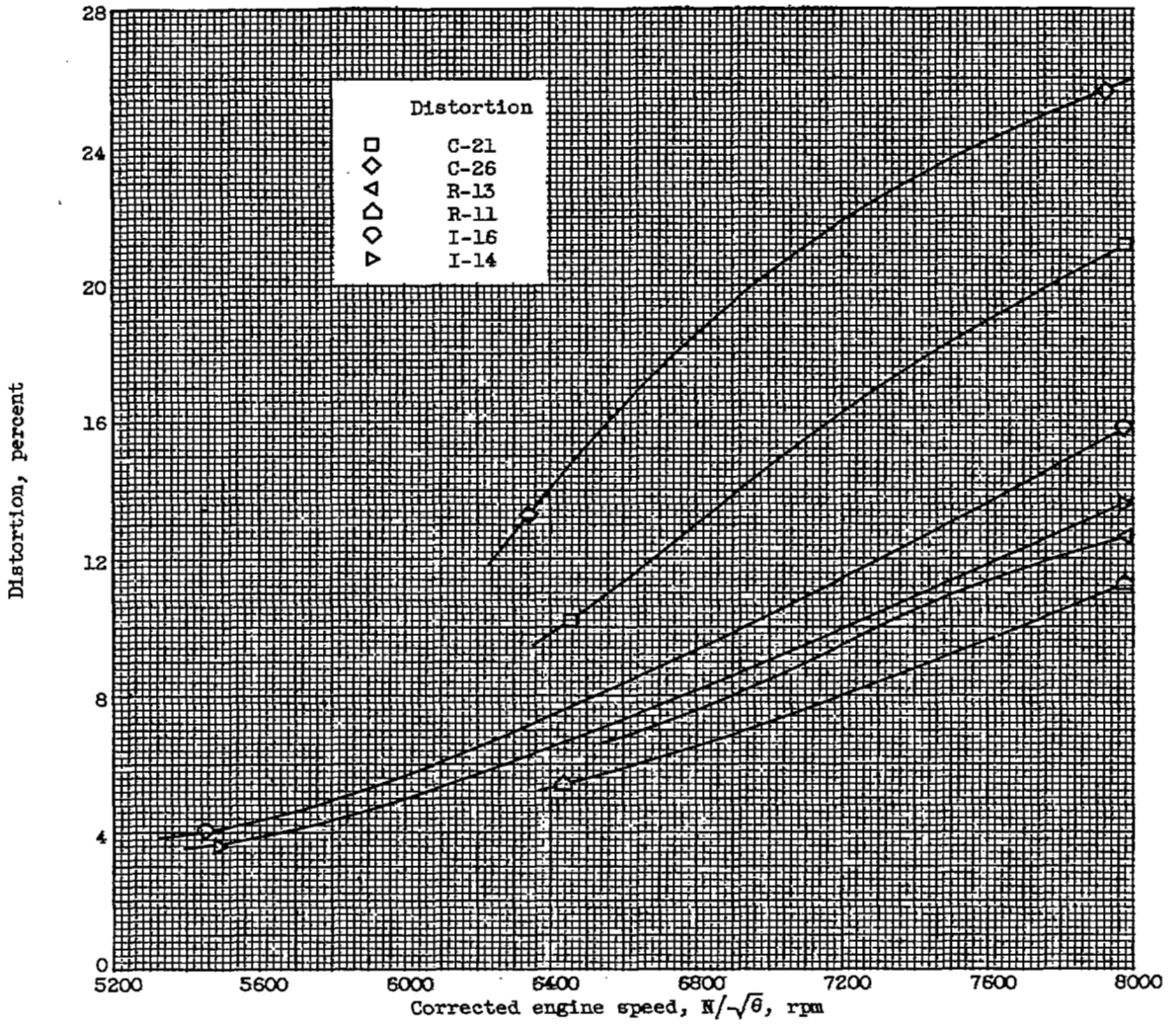

Figure 6. - Variation of distortion with engine speed. Inlet guide vanes open; altitude, 35,000 feet.

[redacted]

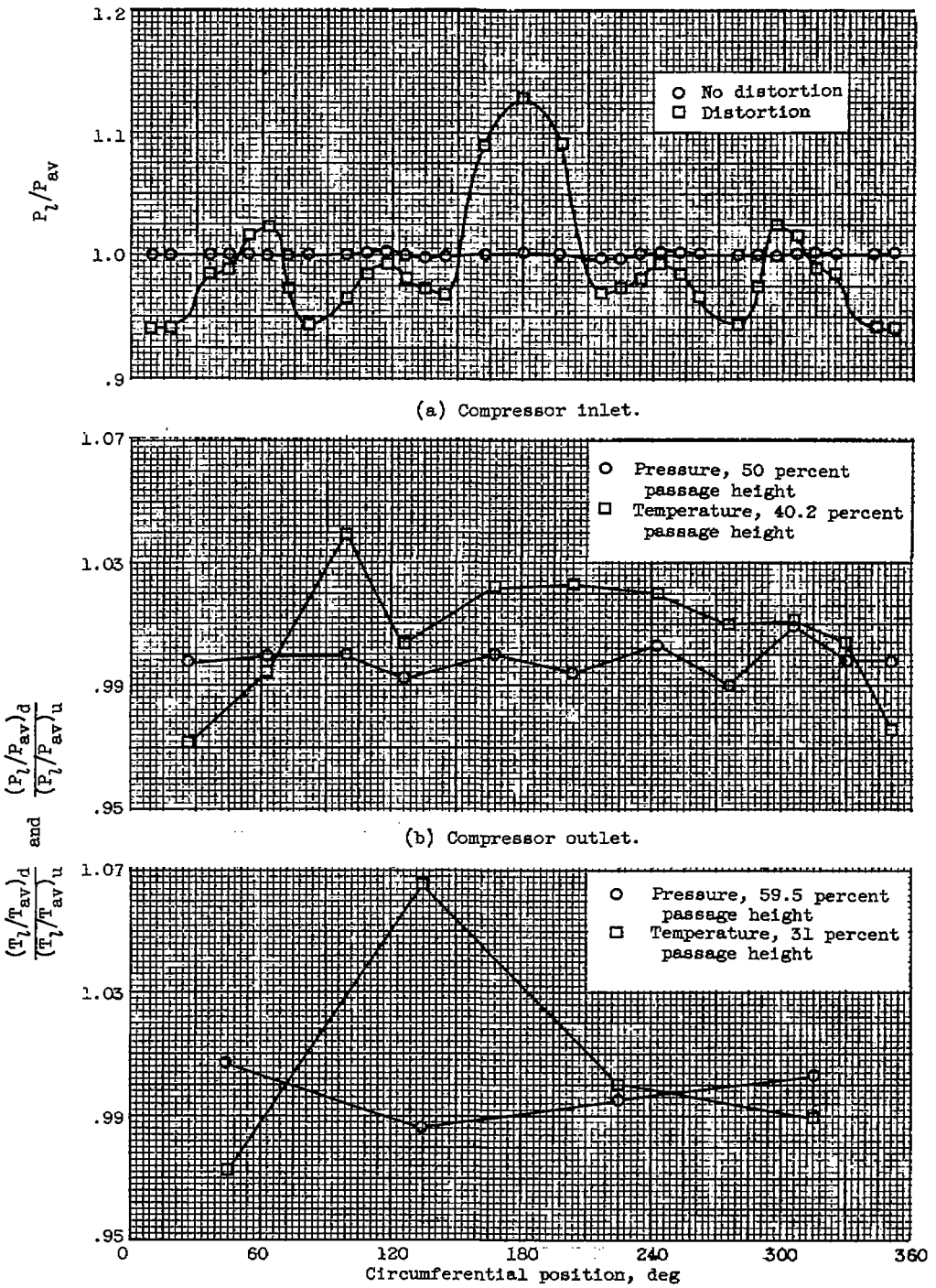

Figure 7. - Typical effects of circumferential distortion on pressure and temperature patterns. Rated engine speed; rated exhaust nozzle; open inlet guide vanes.

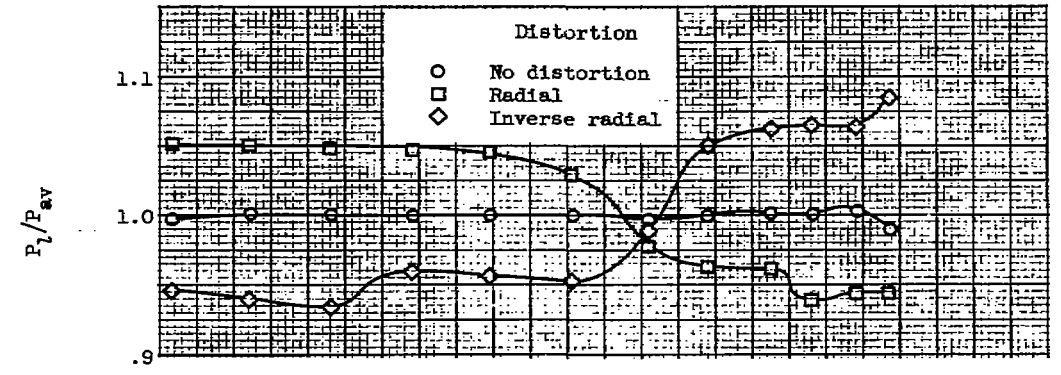

(a) Compressor inlet.

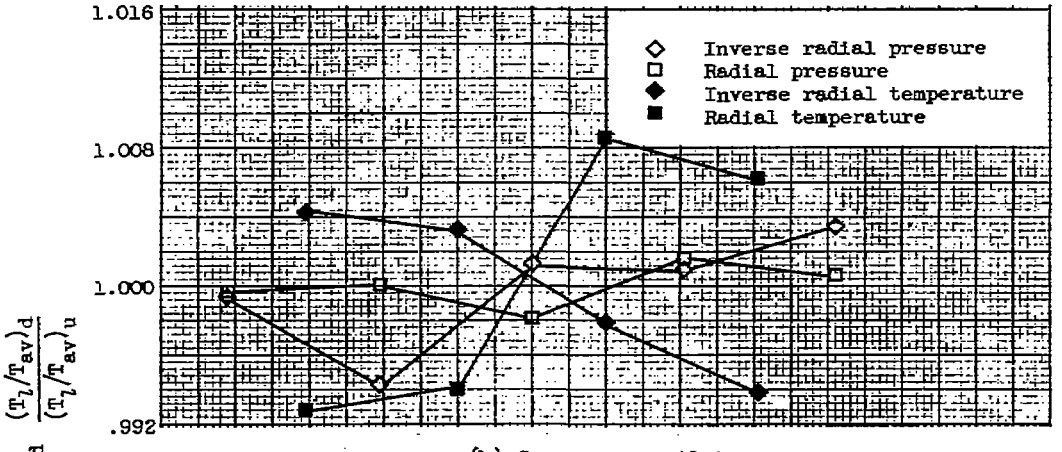

(b) Compressor outlet.

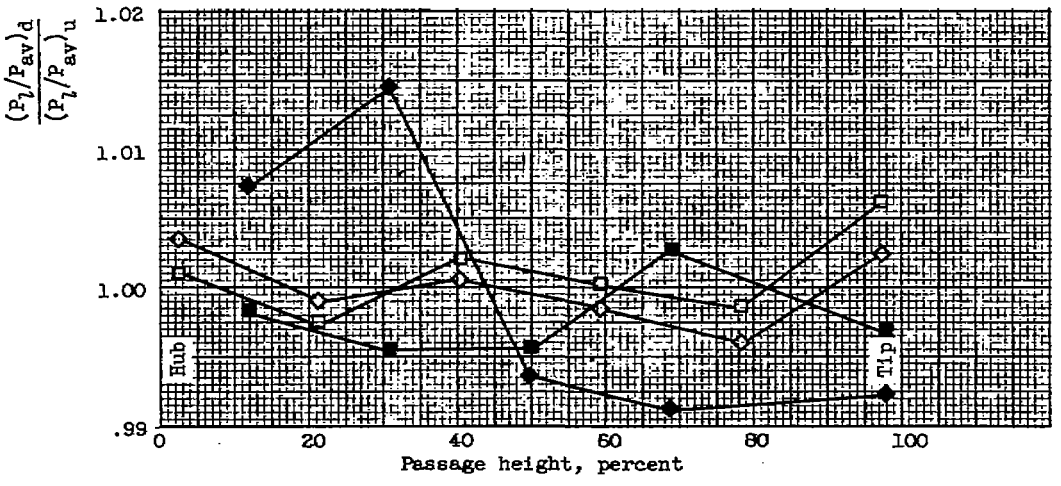

(c) Turbine outlet.

Figure 8. - Typical effects of radial and inverse distortions on pressure and temperature patterns. Rated engine speed; rated exhaust nozzle; open inlet guide vanes.

[redacted]

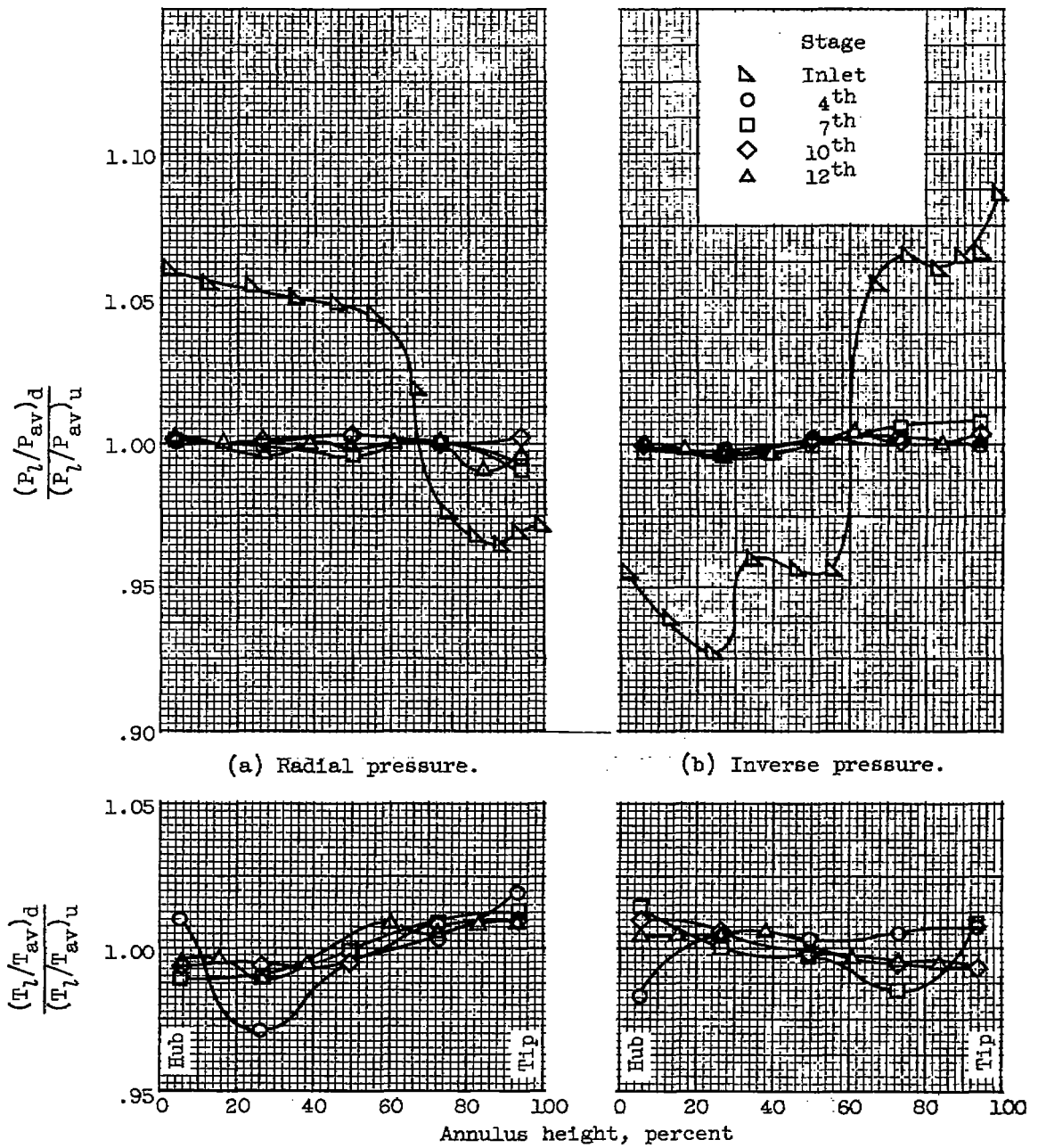

Figure 9. - Typical effects of radial and inverse distortions on compressor-interstage pressure and temperature.

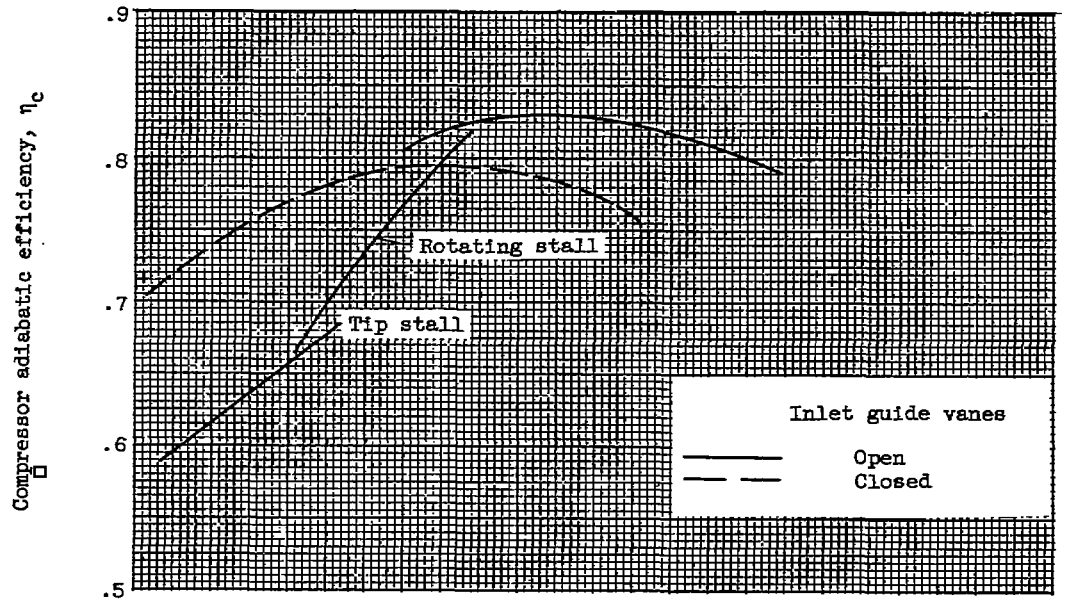

(a) Efficiency.

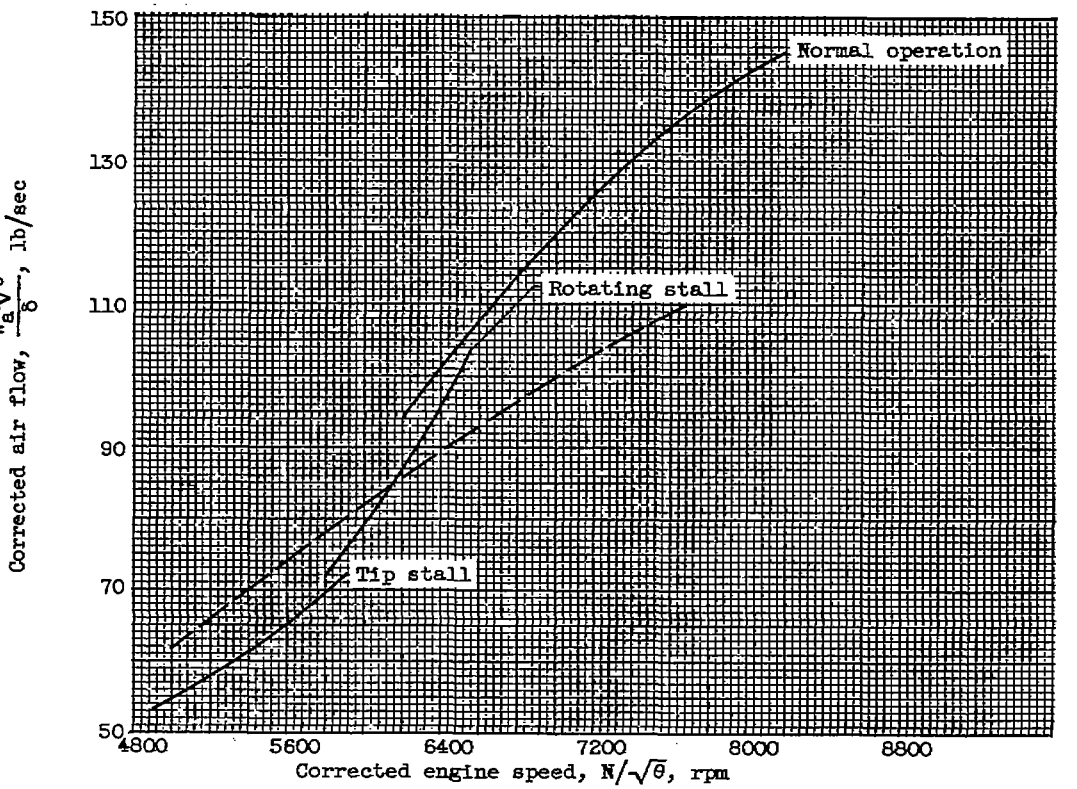

(b) Air flow.

Figure 10. - Typical characteristics of compressor with no distortion (ref. 7).

[redacted]

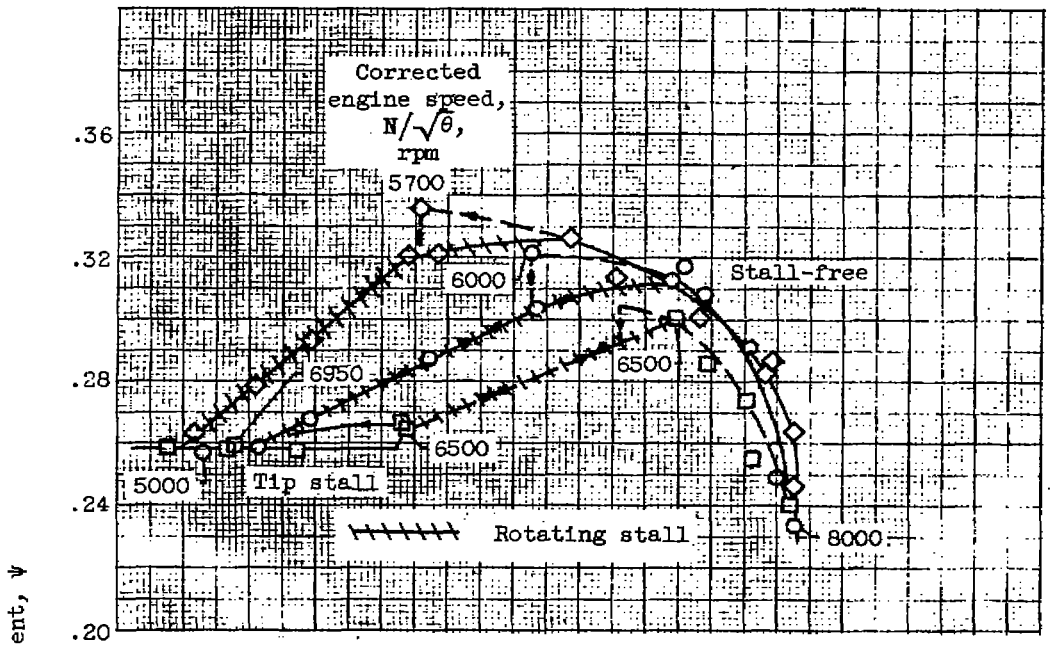

(a) Inlet guide vanes open.

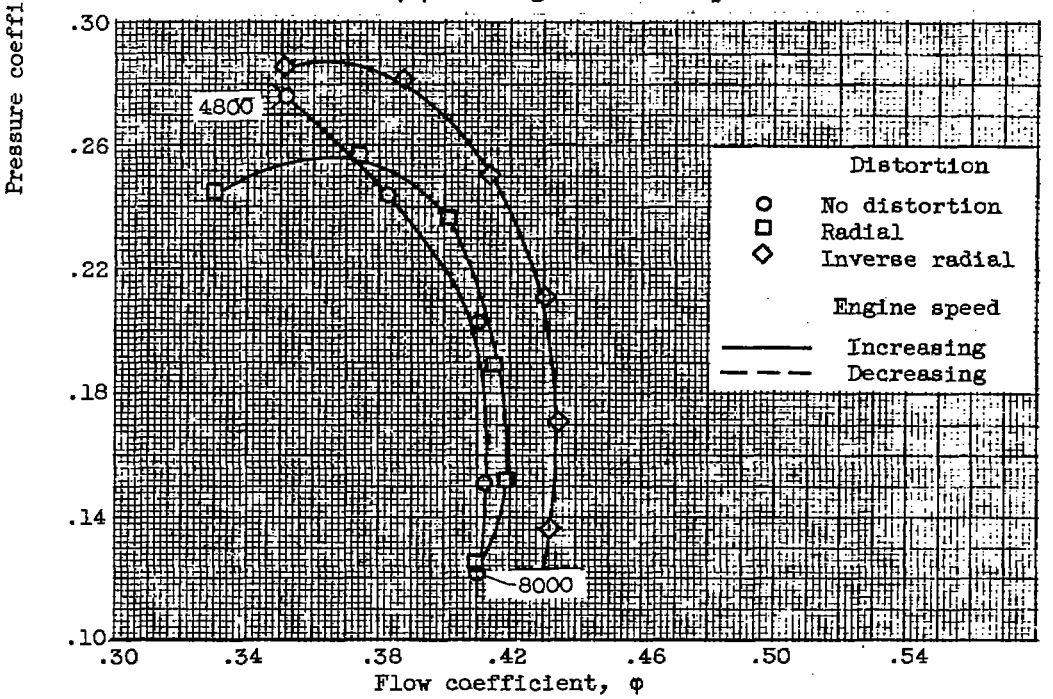

(b) Inlet guide vanes closed.

Figure 11. - Effect of radial and inverse distortions on characteristics of stage groups 1 to 4. Altitude, 35,000 feet; flight Mach number, 0.8.

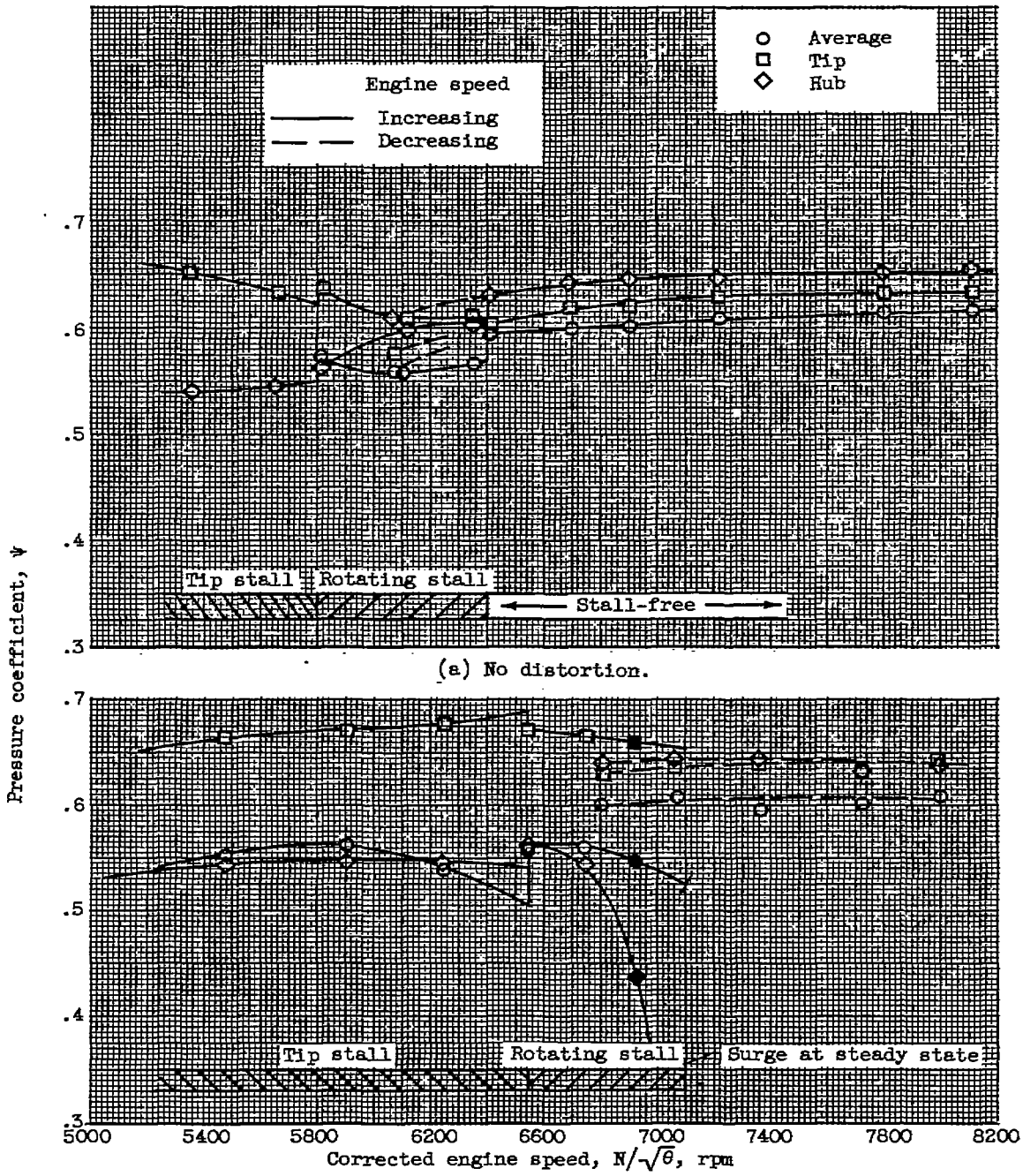

(a) No distortion.

(b) Radial distortion.

Figure 12. - Effect of radial distortion on characteristics of stages 8 to 10. Inlet guide vanes open; altitude, 35,000 feet; flight Mach number, 0.8.

[redacted]

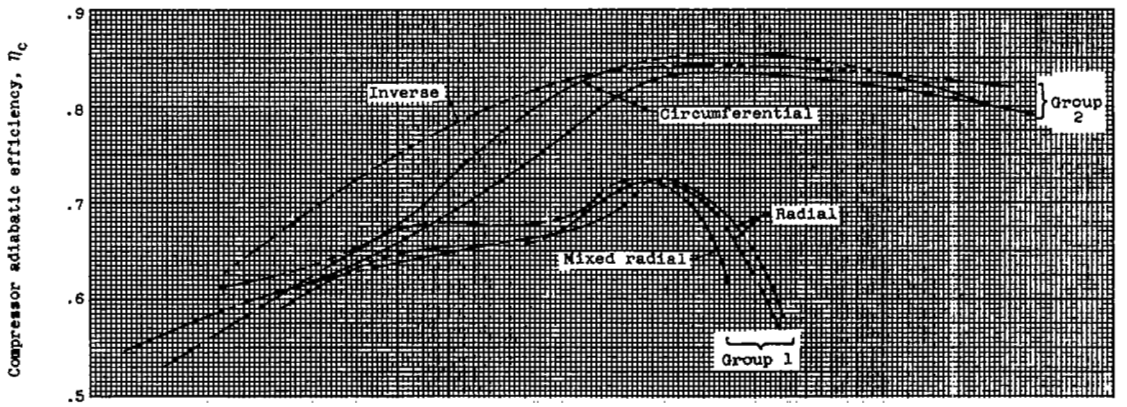

(a) Efficiency. Data taken in direction of increasing speed.

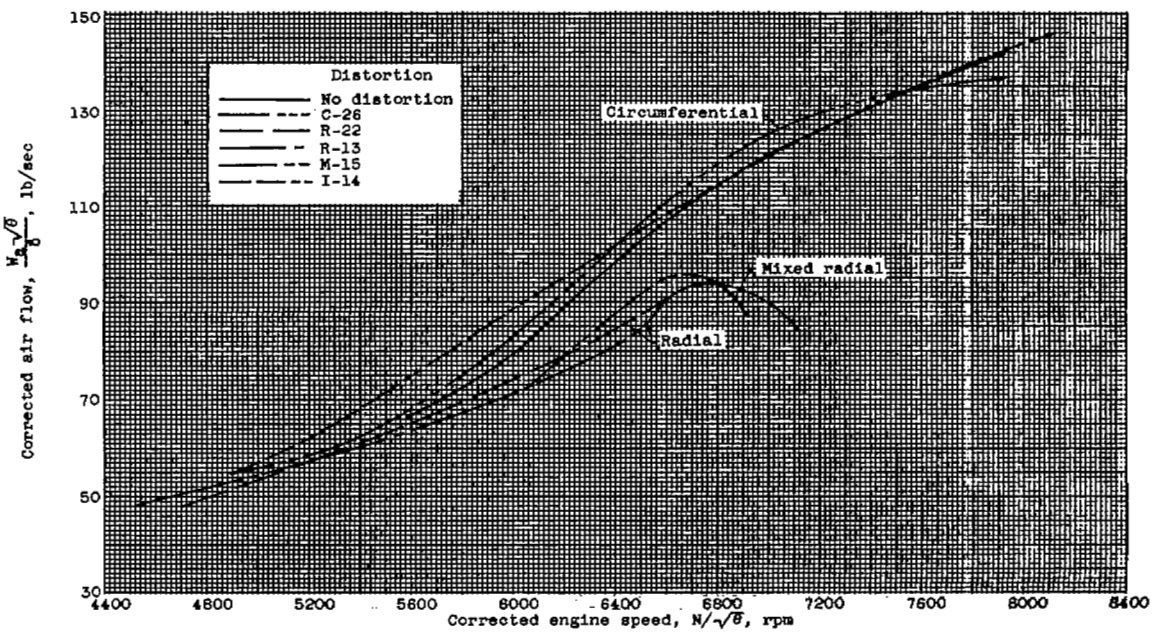

(b) Air flow. Data taken in direction of increasing speed.

Figure 13. - Effect of radial, circumferential, and inverse distortions on compressor efficiency and air flow. Inlet guide vanes open; altitude, 35,000 feet; flight Mach number, 0.8.

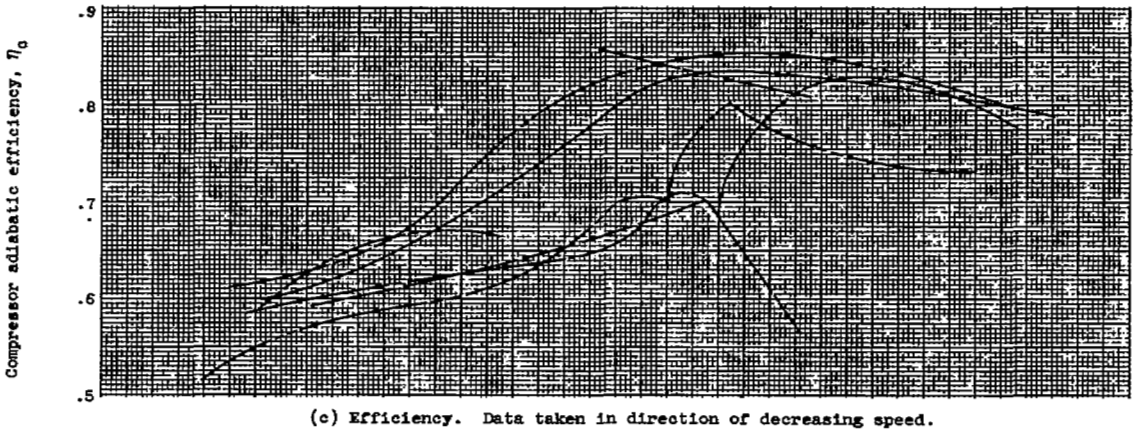

(c) Efficiency. Data taken in direction of decreasing speed.

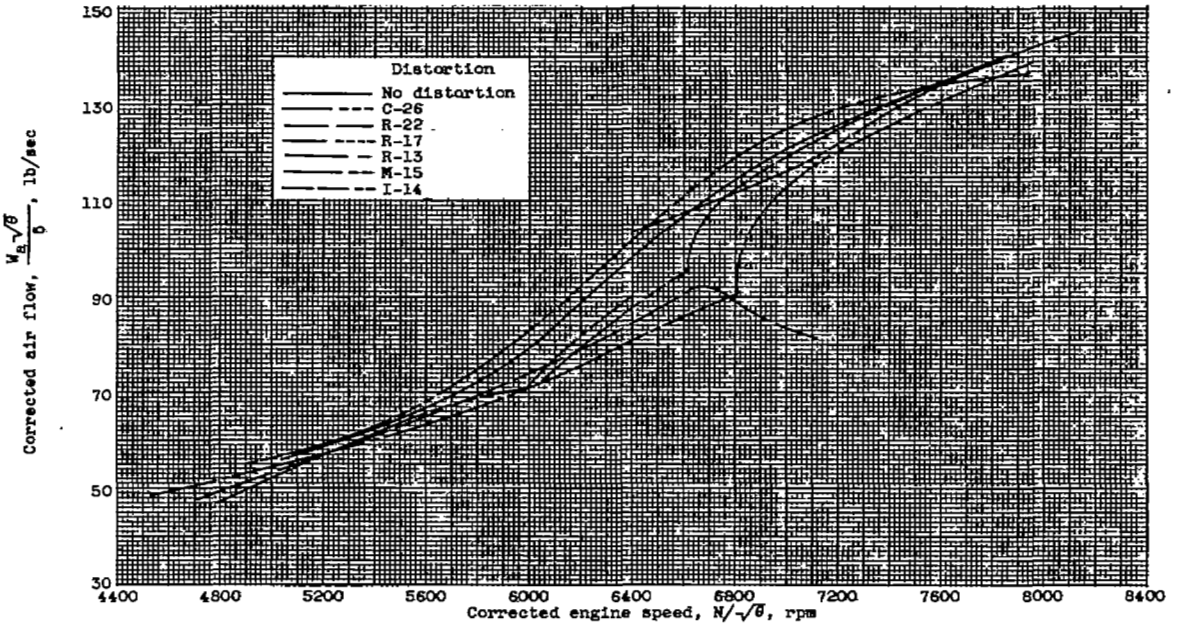

(d) Air flow. Data taken in direction of decreasing speed.

Figure 13. - Concluded. Effect of radial, circumferential, and inverse distortions on compressor efficiency and air flow. Inlet guide vanes open; altitude, 35,000 feet; flight Mach number, 0.8.

[redacted]

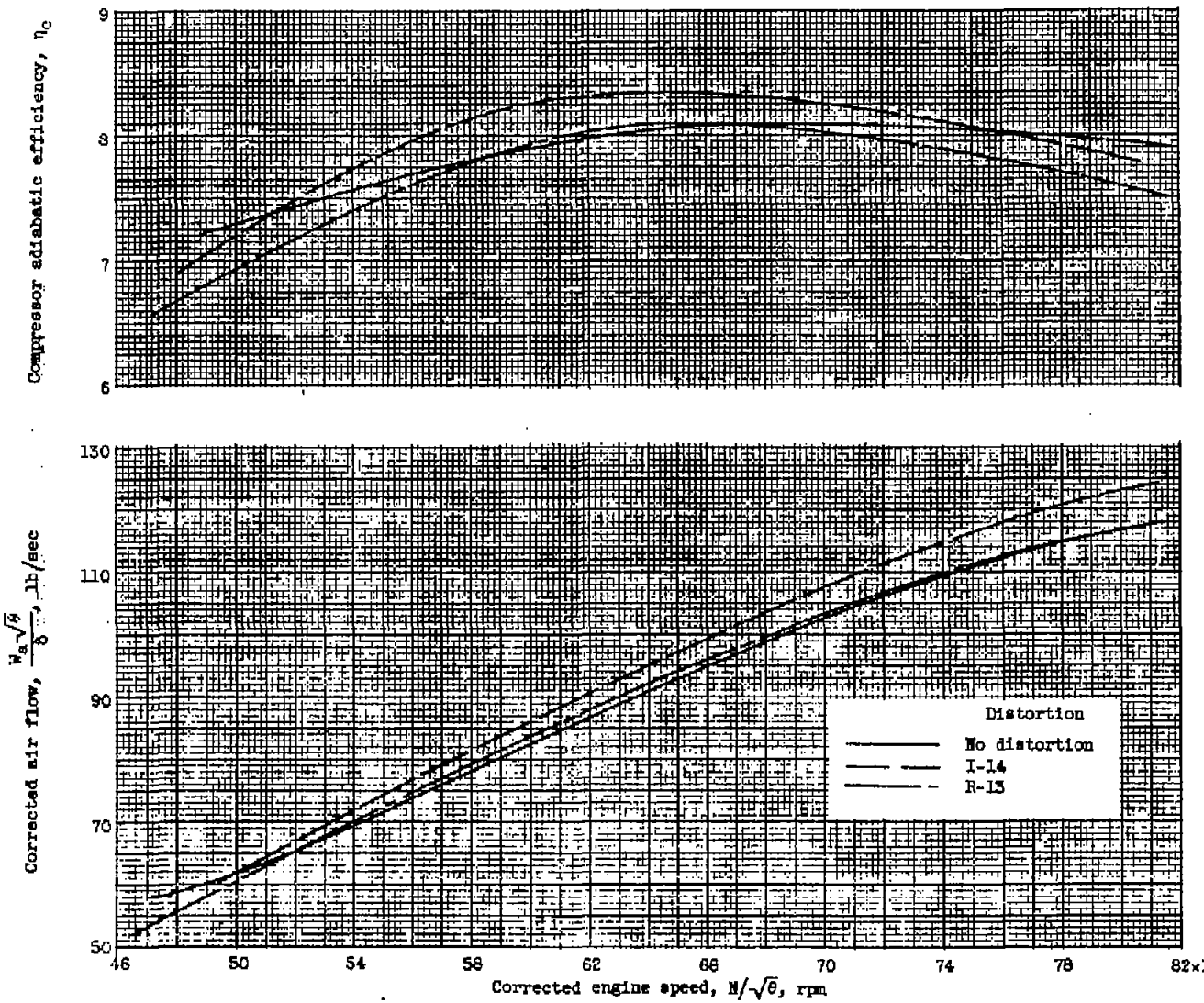

Figure 14. - Effect of radial and inverse distortions on several performance variables. Inlet guide vanes closed; altitude, 35,000 feet; flight Mach number, 0.8.

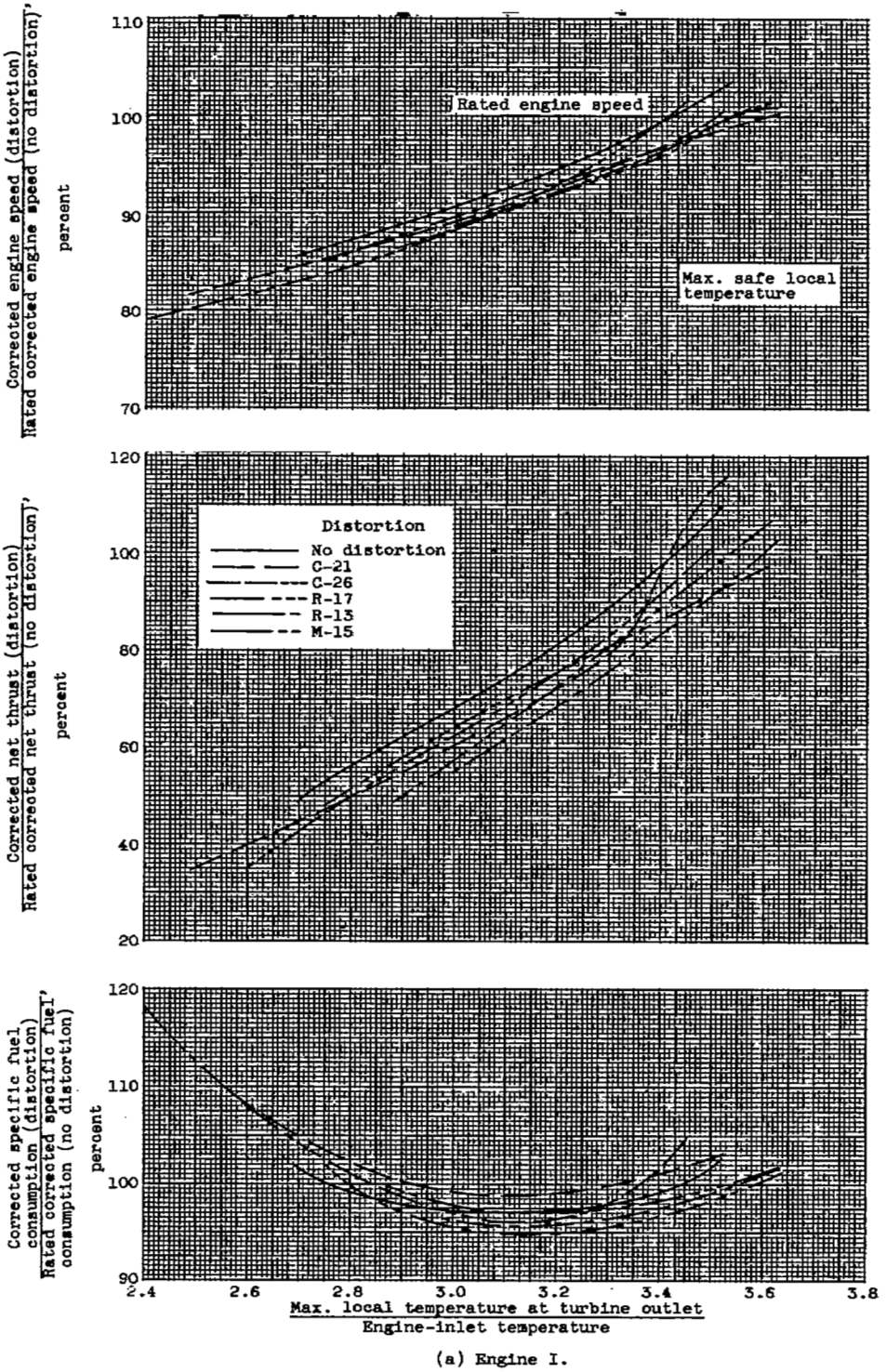

(a) Engine I.

Figure 15. - Effect of distortions on performance at maximum thrust as limited by local temperatures at turbine outlet. Altitude, 35,000 feet; flight Mach number, 0.8.

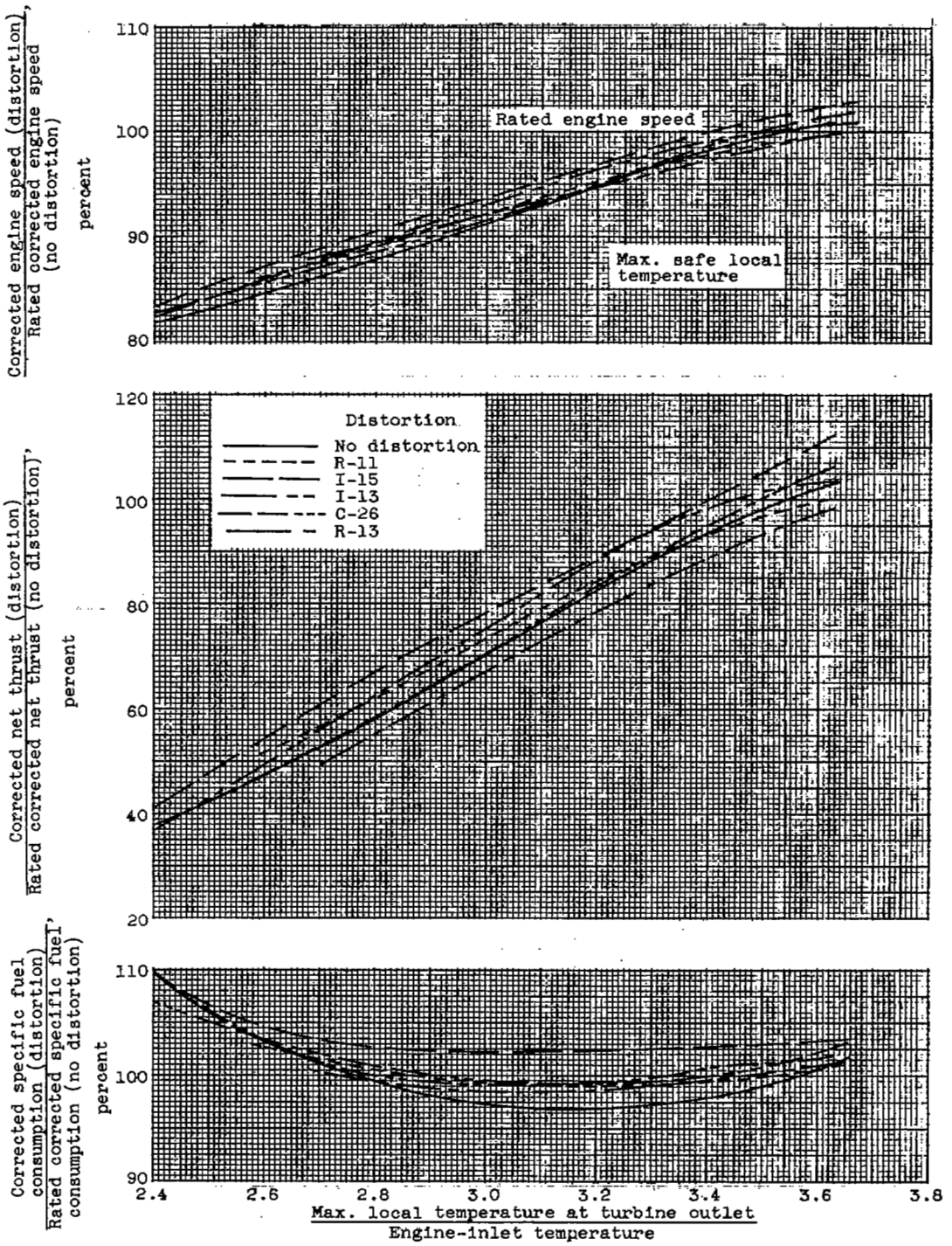

(b) Engine II.

Figure 15. - Concluded. Effect of distortions on performance at maximum thrust as limited by local temperatures at turbine outlet. Altitude, 35,000 feet; flight Mach number, 0.8.

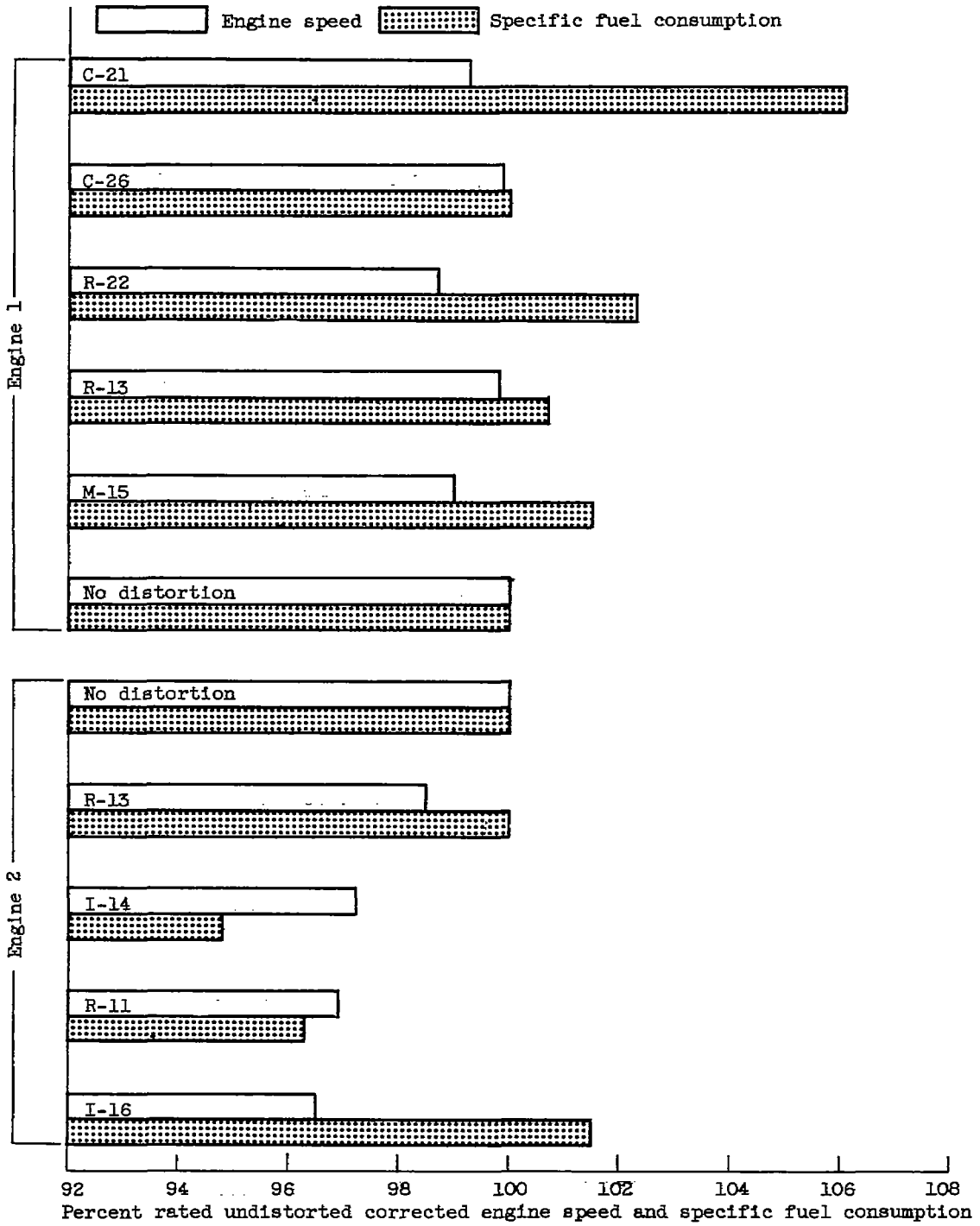

Figure 16. - Effect of distortion on specific fuel consumption at a loiter condition of 30 percent of rated thrust (no distortion).

[redacted]

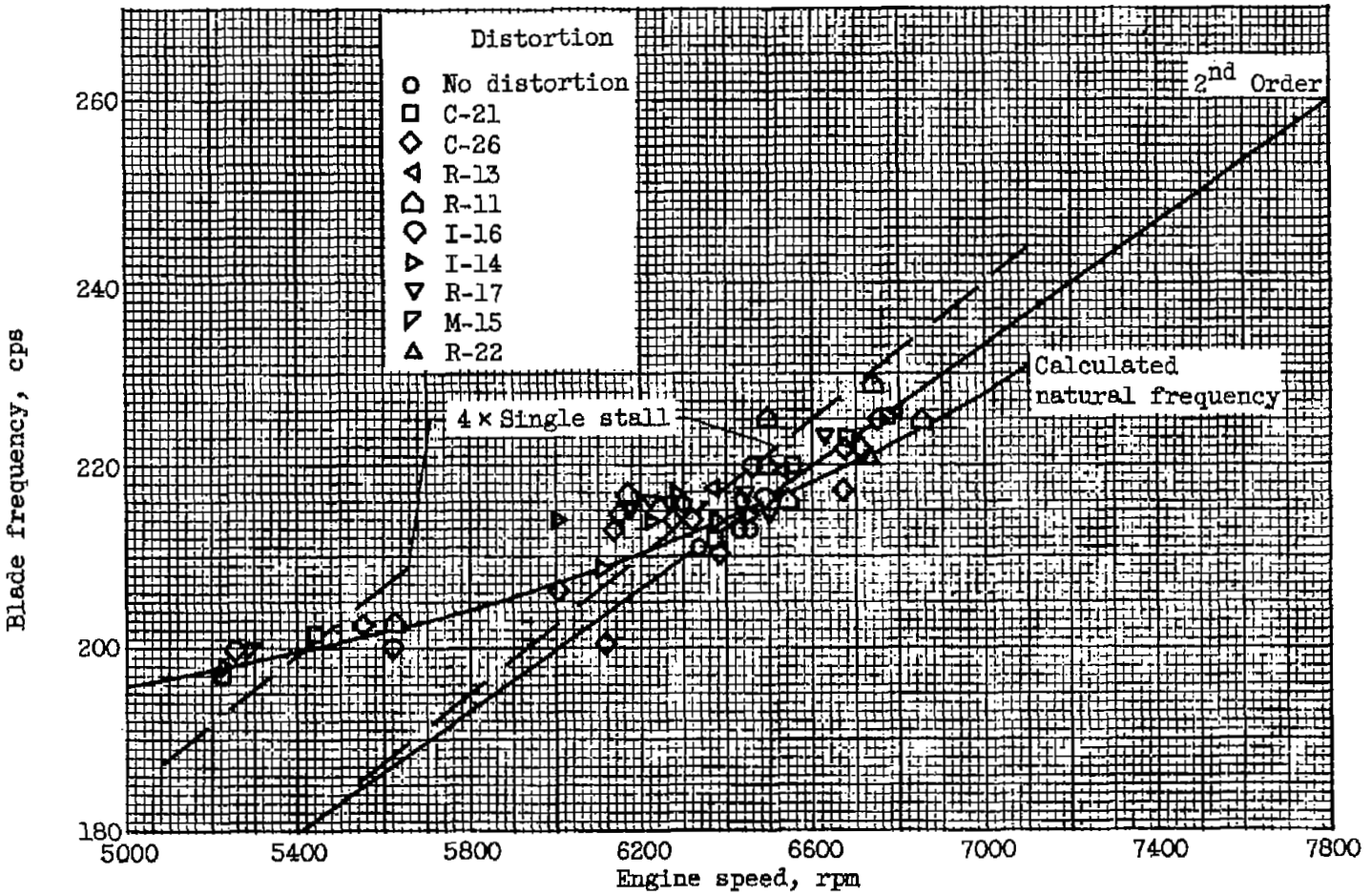

Figure 17. - Occurrence of first-stage rotor-blade vibration as excited by engine order and rotating stall.

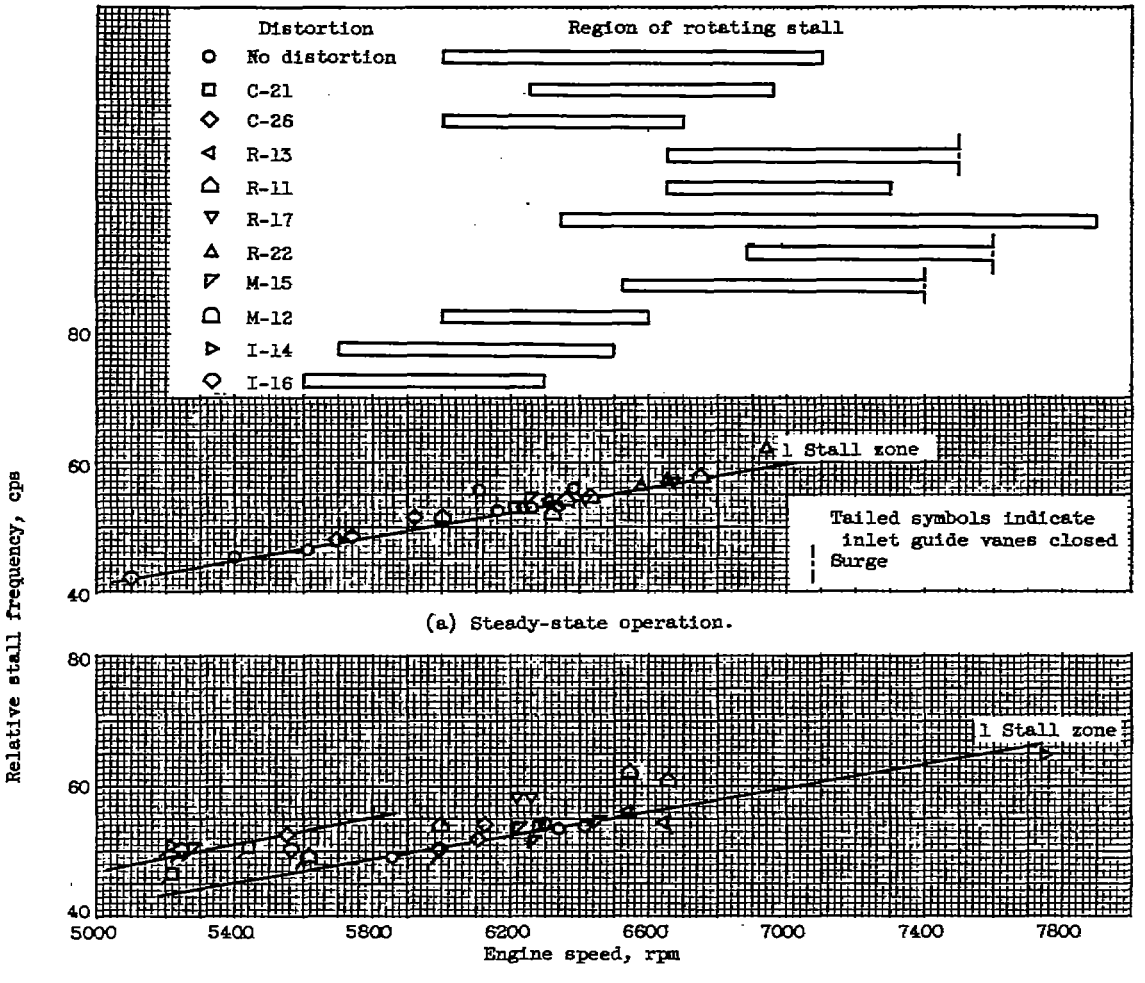

(a) Steady-state operation.

(b) Transient operation.

Figure 18. - Variation of relative stall frequency with rotor speed. Inlet guide vanes open.

[redacted]

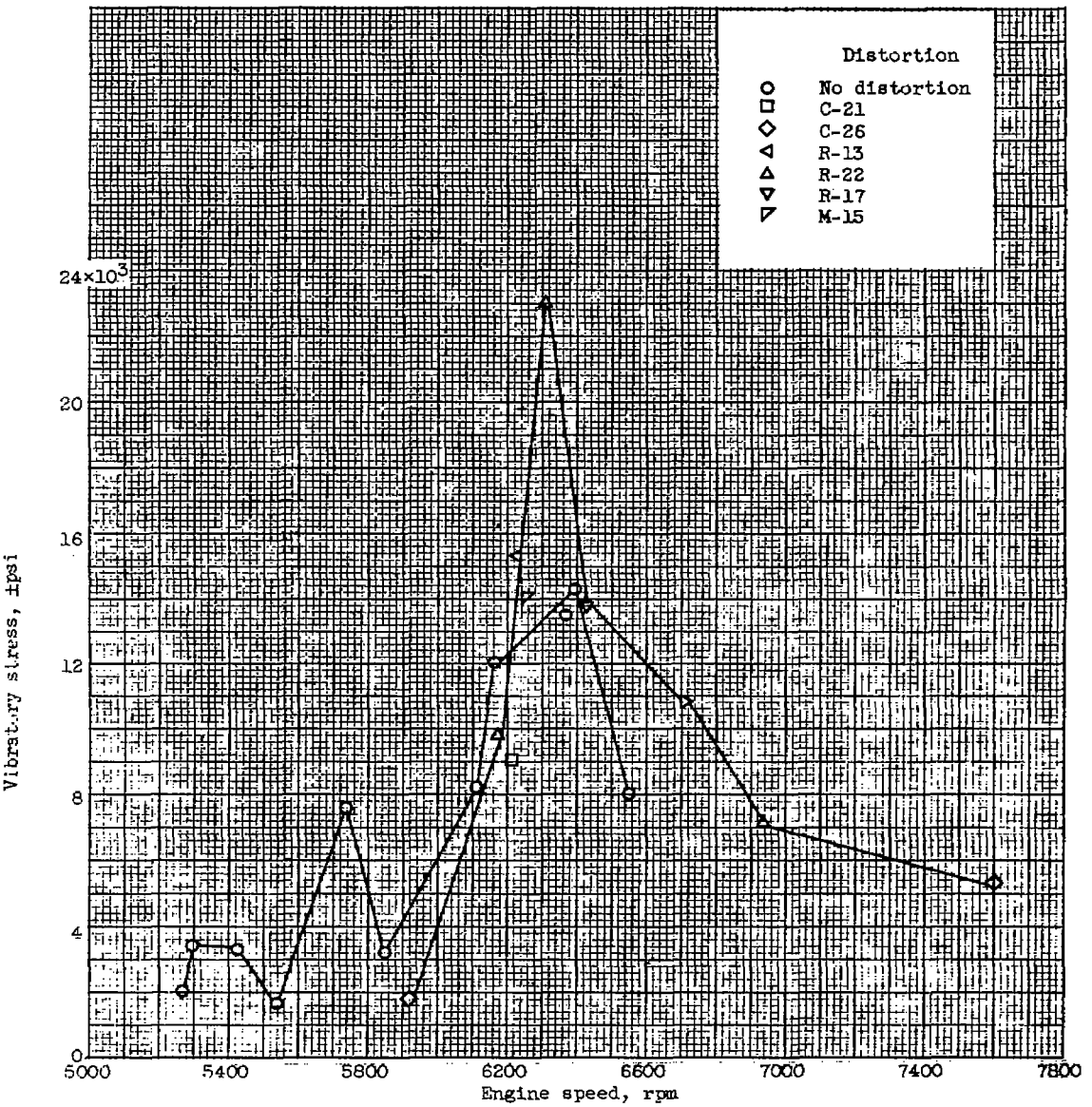

(a) Steady-state operation. Inlet guide vanes open.

Figure 19. - Peak vibratory stress of first-stage rotor blade.

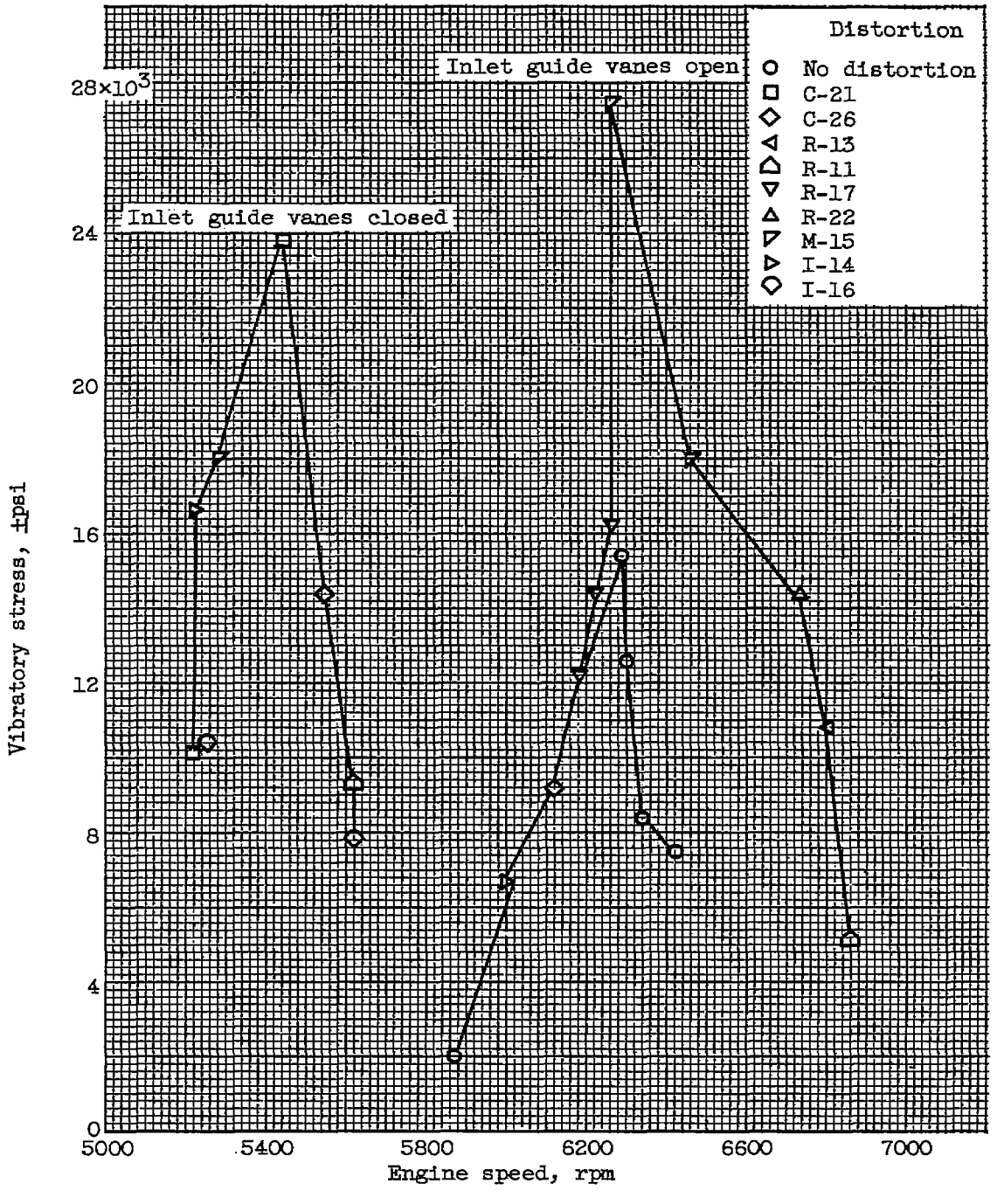

(b) Transient operation.

Figure 19. - Concluded. Peak vibratory stress of first-stage rotor blade.